



Pre-swirl fins design for improved propulsive performances: application to fast twin-screw passenger ships

Stefano Gaggero¹ · Mattia Martinelli¹

Received: 13 March 2022 / Accepted: 20 July 2022 / Published online: 13 August 2022
© The Author(s) 2022

Abstract

Pre-swirl fins-based energy saving devices (ESDs) have been designed to improve the propulsive performances of twin-screw ships. To this aim, a combined BEM/RANSE method for efficient self-propulsion prediction is required. The approach is included in a framework for a design by optimization, where systematic variations of the ESD geometry have been used to explore the design space and maximize the energy-saving effect of the device. Surrogate models based on Ordinary Kriging are used too, with the aim of realizing an affordable design workflow for the very preliminary design of such devices. The results show encouraging improvements that reach promising energy-savings up to 3% at the design point and satisfactory savings also in off-design functioning conditions.

Keywords Energy saving devices · Pre-swirl stators · Optimization · Design by optimization · SBDO

1 Introduction

The progressive application of stricter environmental regulations, such as the EEDI and the EEOI indexes (IMO 2009a, b; 2014), has imposed and will soon impose substantial and progressive reductions in the gaseous emissions of pollutants. Combined with the necessity to reduce the ship operative costs (i.e. fuel), this regulatory framework represents one of the most important drivers in the ships innovation, with obvious consequences also in the development of their propulsion systems. Energy saving devices (ESDs) fall into this innovation process. These are “simple” and cost-effective solutions capable of improving the overall propulsive efficiency of the ship as a whole: WED, PBCF, pre- and post-swirl stators, as well as highly efficient non-conventional propellers (Lammeren 1949; Ouchi and Ogura 1988; Kim et al. 2004; Andersen et al. 2000), are some of the recently proposed solutions that have been developed to recover some of the hydrodynamic losses of the propulsion system, for both new

projects and retrofits. Some devices act to reduce the propeller load, others to realize a positive interaction with the stern flow of the ship, or to reduce the losses due to strong propeller tip and hub vortexes. Pre-swirl stators, which are the subject of the current study, belong to the class of energy-saving devices devoted to recover the propeller rotational losses.

Pre-swirl stators consist of multiple fins installed in front of the propeller to induce a swirl inflow to the propeller itself in the opposite direction of its rotation, straightening the final wake. This swirling flow produces a “free” additional load on propeller blades at constant absorbed torque, decreasing the rate of rotation (consequently the delivered power) needed to achieve the desired ship speed. Since the first application of these ESDs, literature results have shown very promising saving effects. In the framework of the EU project GRIP (Streckwall and Xing-Kaeding 2017; Schuiling and van Terwisga 2017; Prins et al. 2016), pre-swirl stators reached an energy-saving of 6%, that in the particular case of a twin-screw passenger vessel was close to 4%. Koushan et al. (2020) developed pre-swirl stators for a chemical tanker and their numerical results, claiming a power savings of 2.5%, were confirmed during a dedicated model-scale experimental campaign. The usage of flapped and “controllable” pre-swirl stators was proposed to cope with non-constant operative conditions (slow steaming, fouling, weather, change of draft) and to ensure the highest possible energy-saving, which

✉ Stefano Gaggero
stefano.gaggero@unige.it

Mattia Martinelli
mattia.martinelli@edu.unige.it

¹ Department of Naval Architecture, Electrical, Electronic and Telecommunication Engineering, University of Genoa, Via Montallegro 1, 16145 Genoa, Italy

reached a shaft power reduction of 4% in the case of a bulk carrier (Nielsen and Jin 2019). Since pre-swirl fins always create resistance, a positive net gain is possible only if the additional thrust (provided by the propeller operating in the wake of the pre-swirl stator) is higher than the resistance added to the ship by the presence of the fins themselves. This aspect must be considered in the design process, selecting for instance merit indexes that are able to simultaneously account for the positive effect of the device and its side effects (flow separation and vortex shedding). The usual application of pre-swirl stators mainly to slow and fully-blocked ships exactly considers this necessity, since for them the added resistance of these appendages (working in the decelerated flow at the stern) is small compared to the recovery action on the rotational flow exerted by the device.

These considerations sustain the need for dedicated design methodologies capable of embracing conflicting objectives (in this case a balance between energy saving effect and the associated additional resistance that can nullify it) and able to deal with the complexity of the problem. The nature of these ESDs potentially requires each fin to be designed to meet the local characteristics of the flow, which is, in turn, influenced by the induced velocities of the propeller in self-propulsion functioning. Opportune design criteria (reduction of the shaft power or reduction of the ship resistance) must be selected to adequately consider the hull/ESD/propeller system as a whole. Moreover, full-scale analyses are mandatory since Reynolds effects can substantially change the flow field and the resulting optimal configuration of the device. Simulation-based design optimization methods, as those already applied for propeller or other ESDs designs (Gaggero 2020; Furcas et al. 2020) represent a solid approach to deal with these needs, and successful results in the case of Pre-Swirl Stator fins have been already achieved using these approaches even if in the more usual case of fully-blocked and slow ships (Furcas and Gaggero 2021). SBDO, indeed, allows for systematic explorations of enlarged design spaces using the appropriate solvers (RANSE and/or coupled BEM/RANSE) mandatory for the characterization of the pre-swirl functioning. Combined with parametric representations of the geometry and optimization algorithms they can easily turn into flexible and effective design methods.

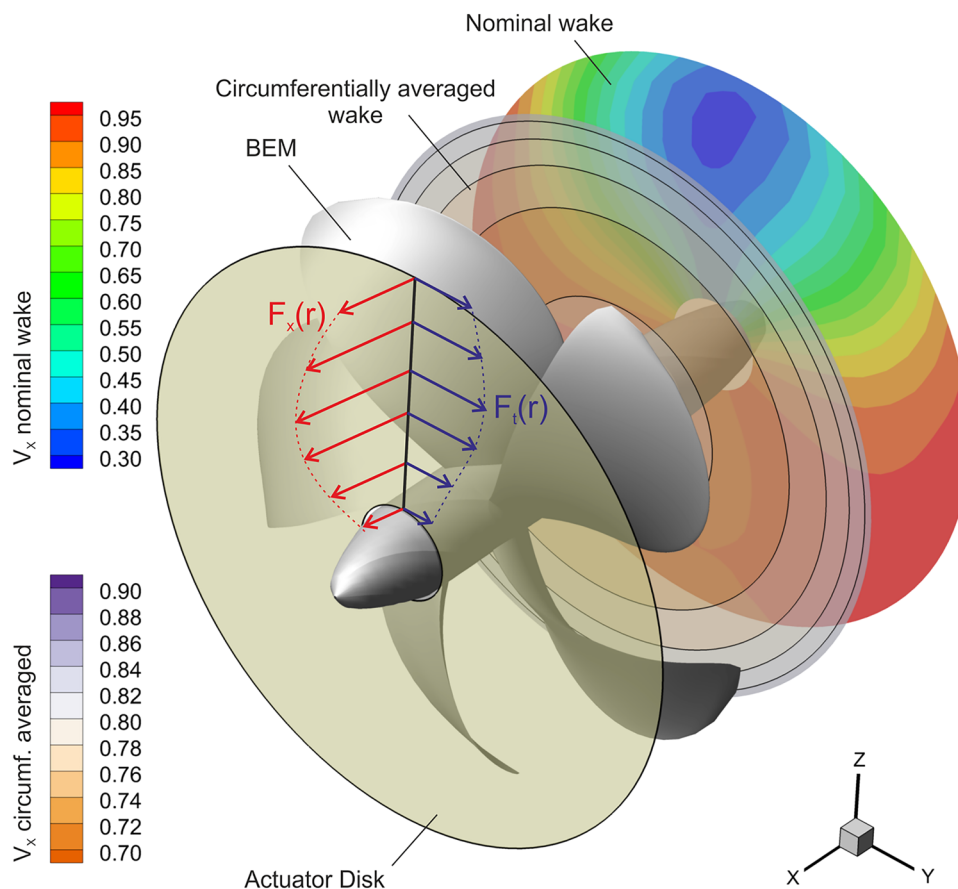
This is precisely the design approach selected in this work. Particularly, the design activity focuses on pre-swirl stators applied to two relatively small and fast twin-screw passenger ships (with different shaft brackets arrangements) that for their nature represent a demanding application case for pre-swirl devices. The SBDO approach involves a simplified self-propulsion estimation method, based on the results of Gaggero et al. (2018) and Villa et al. (2019) using a combination of BEM and RANSE calculations, eventually exploited through appropriate surrogate models. The results are the optimal pre-swirl fins parameters ensuring at the same

time appreciable energy savings (measured as a delivered shaft power reduction) without (excessive) worsening the side effects (i.e. risk of cavitation) of the propeller. Energy savings, close to 3% at the design point but also at selected off-design functioning conditions, are finally verified using self-propulsion calculations based on fully resolved RANSE analyses.

2 Coupled BEM/RANSE for simplified self-propulsion estimations

The accurate characterization of pre-swirl appendages, that needs self-propulsion estimation of the incoming inflow and of the propeller functioning, requires ad-hoc tools to be included in a computationally efficient manner into a simulation-based design optimization approach. Pre-swirl stators, indeed, realize a substantially interaction with the propeller since they change the inflow to the propeller itself to reduce the shaft power at which the required thrust is delivered. On the other hand, their optimal shape to avoid flow separation and excessive fins resistance, nullifying the possible saving, depends on the induced flow filed by the propeller itself. Then, a reliable estimation of the recovery effect is possible only by the characterization of the entire propulsion system (the propeller and the ESD) working with the effective wake. This prevents the use of simplified actuator disk models only, which can solely provide a very crude estimation of the propeller functioning point, in favor at least of coupled BEM/RANSE methods that are necessary, instead, for decent propeller performances estimation. While a decent estimation of the thrust deduction factor, indeed, is possible using actuator disks, they completely ignore the current, unsteady, functioning of the propeller. If, in a certain measure, an estimation of the propeller rate of revolution is possible by using its open water curves, some auxiliary variables (K_T/J^2) and very simplified estimations of the wake fraction, a method capable of accounting for the tangential components of the effective wake modified by the pre-swirl on the propeller loading and unsteady functioning is required. Most of the saving effects of this ESD, indeed, relies on the modification of the tangential flow field to the propeller. A self-propulsion estimation approach capable of accounting of these modifications is consequently required to assess the merit of the Pre-Swirl system. Since the computational efficiency is the bottleneck of any SBDO, for this design activity a BEM/RANSE coupling method further simplified with respect to that proposed in Gaggero et al. (2017) is required. In current approach RANSE analyses characterize the velocity and the pressure field at the stern of the ship by employing an actuator disk in place of the propeller. An unsteady BEM, instead, is in charge of the calculations of the propeller functioning (absorbed power) under the resulting

Fig. 1 Averaging process for the characterization of the momentum source of the actuator disk. The nominal wake is transformed in a circumferentially averaged wake. Equivalent open water BEM analyses using this averaged wake realizes the axial and tangential radial load distribution of the actuator disk



spatial non-uniform effective wake. The coupling between the two solvers is weak since it relies on an approximated effective wake evaluated from the ship nominal one, not iteratively updated (i.e. self-induced velocities at any propeller rps guess) and not accounting for the unsteady and spatial non-uniform nature of the interaction, considered instead in more advanced body force methods (Gaggero et al. 2017). This approximation, successfully exploited for fully-blocked ships (Furcas and Gaggero 2021; Gaggero et al. 2018; Villa et al. 2019) makes the optimization computationally feasible.

In particular, momentum sources replace the propeller at the stern of the ship, in terms of pressure (for the evaluation of the thrust deduction) and velocity (for the evaluation of the wake fraction) disturbance inside the RANSE calculations. These sources are proportional to the radial distributions of circumferentially constant axial and tangential loads which are those obtained by preliminary steady BEM calculations of the propeller working in the circumferentially averaged nominal wake of the ship (Fig. 1). The corresponding total wake on the propeller plane due to the presence of the actuator disk is then elaborated to derive the effective wake for the unsteady propeller functioning. The same actuator disk used for self-propulsion (i.e. the same radial distribution of axial

and tangential load), when delivering the same thrust in a uniform flow with velocity equal to the averaged nominal wake measured during towing tests, provides a radially varying and circumferentially averaged velocity field that satisfactorily represents the propeller self-induced velocities. With this assumption, the self-induced velocities under the effective wake are approximated as those produced by the propeller under the nominal wake. Since the propellers (the actuator disks) under both wakes (self-propulsion with the actuator disk behind the ship and these equivalent “open water” analysis using the opportune undisturbed flow velocity) deliver the same thrust using the same spatial distribution of load, this approximation seems plausible in the context of these simplified calculations. Without any of the BEM/RANSE iterations required by more sophisticated approaches, then the effective wake can be calculated as:

$$V_{\text{effective}}^{\text{ship}} = V_{\text{total}}^{\text{ship}} - \left(V_{\text{total}}^{\text{disk}} - V_{\text{ship}} \cdot (1 - w)_{\text{nominal}} \right) \quad (1)$$

where:

- $V_{\text{total}}^{\text{ship}}$ is the “total” velocity field (Carlton 2007) computed by RANSE in self-propulsion condition on the propeller plane with the influence of the actuator disk;

- $V_{\text{total}}^{\text{disk}}$ is the “total” velocity field on the propeller plane of an open water analysis where the actuator disk, loaded with the same distribution used in behind ship condition and delivering the same thrust of self-propulsion condition, is subjected to a uniform inflow equivalent to the averaged nominal wake of the ship (i.e., $V_{\text{ship}} \cdot (1 - w)_{\text{nominal}}$);
- V_{ship} is the ship velocity;
- $(1 - w)_{\text{nominal}}$ is the nominal wake fraction in towing condition;

Since the mutual interactions between the wave pattern and the pre-swirl appendages can be considered negligible, at least in the preliminary design phase, an additional simplification for the self-propulsion estimation concerns the calculation of the current ship resistance (i.e., in presence of the ESD) starting from the double-model assumption, as successfully done in many similar cases (Gaggero et al. 2017; Koushan et al. 2020). A “constant” wave resistance contribution, i.e., independent of the propeller working condition and ESD, can be computed by subtracting the double model drag to the total hull resistance calculated in towing conditions with the free surface. This estimation includes the pure wave resistance and all the double-model approximations such as the variation of the wetted surface for the reference ship. By adding it to the current drag of the double model equipped with ESD and propellers (or equivalent actuator disks), a reasonable estimation of the total hull drag is possible, allowing for cost-effective self-propulsion predictions.

Under these simplifications, the complete coupling algorithm that realizes the self-propulsion prediction is outlined in the flow chart of Fig. 2. The process is described in the most general case that includes the pre-swirl stators but obviously applies also for the bare hull. The objective of the process is the estimation of the delivered power of the propeller, which is the objective to be minimized in the design process. To this aim, the evaluation of the ship resistance (i.e., the required propeller thrust) is required at first. This step is realized in Blocks 1 to 3 of the proposed flow chart.

Block 1 considers the double model in towing condition while Block 2 oversees the analyses that account for the action of the propeller (estimation of the thrust deduction factor) using entirely actuator disk calculations that always resulted sufficient (Gaggero et al. 2017; Kim et al. 2004) for this kind of estimations. The simplified treatment of the “wave resistance”, obtained numerically by a dedicated RANSE analysis using multiphase flow and V_0F capabilities, is used in Block 3 to derive the towed and the self-propulsion resistance. In addition to the thrust deduction and the ship resistance in self-propulsion conditions, the outputs of these analyses are the nominal (Block 1) and the total (Block 2) wakes on the propeller plane, which in turn are the inputs needed to assess the propeller self-induced velocities. Block 4 is devoted to this calculation realizing the weak BEM-

RANSE coupling described in Eq. (1). By subtracting the approximated self-induced velocities from the total velocity field obtained in Block 2, the effective wake field can be determined in Block 5. Once the effective wake fraction of the resulting non-uniform field and the thrust deduction factor (from Block 3) are known, also a preliminary propeller rate of revolution can be estimated utilizing the available (numerical or from experiments) propeller open water curves. These are the “first guessed” propeller performances of Block 6. Block 7, finally, is in charge of the unsteady characterization of the propeller using unsteady BEM calculations. It accepts as input the effective wake evaluated in Block 5 (then considering the complete three-dimensional inflow to the propeller, in particular the tangential part of the incoming flow to the propeller, neglected in Block 6), the preliminary estimation of the propeller rate of revolution using open water curves and the target thrust determined by the self-propulsion analysis using the actuator disk. In this case, the effective wake does not change iteration per iteration, as in the case of the computations using iterative and spatially varying body forces approaches, since it is assumed that the simplified actuator disk is equivalent to the unsteady propeller in terms of both (averaged) self-induced velocities and delivered forces. Iterations, instead, are used to tune the propeller rate of revolution accounting for the spatial non-uniformity of the wake and the modification of the tangential components of the inflow caused by the pre-swirl fins. Once the propeller rate of revolution necessary to provide an averaged unsteady thrust equal to the ship resistance in self-propulsion (that of Block 3) has been obtained, the time-averaged delivered power can be determined to assess the performance of the propulsive configuration under investigation.

3 Test cases

The test cases selected for this design activity are two twin-screw, relatively fast, mega-yachts designed by Azimut|Benetti. The first (Ship-1) is a 33 m long ship, originally designed for a displacement of 185 tons and a cruise speed of 16 knots (kn). The final configuration examined in this study account for an updated displacement of 200 tons and a speed of 15 kn. The shaft arrangement (Fig. 3) consists of only one bracket. The second (Ship-2) is 37 m long, 210 tons ship operating at a speed slightly higher than 17 kn. The reference condition for the design, however, was for a ship speed of 14 kn. The shaft arrangement, in this case, consist in the typical “V” shaped configurations using two brackets.

For Ship-1 several measurements, including model scale towing tank tests (with nominal wake measurement) and open water propeller performance, were available and consequently were used to validate the approaches employed in the self-propulsion estimation and then in the optimization

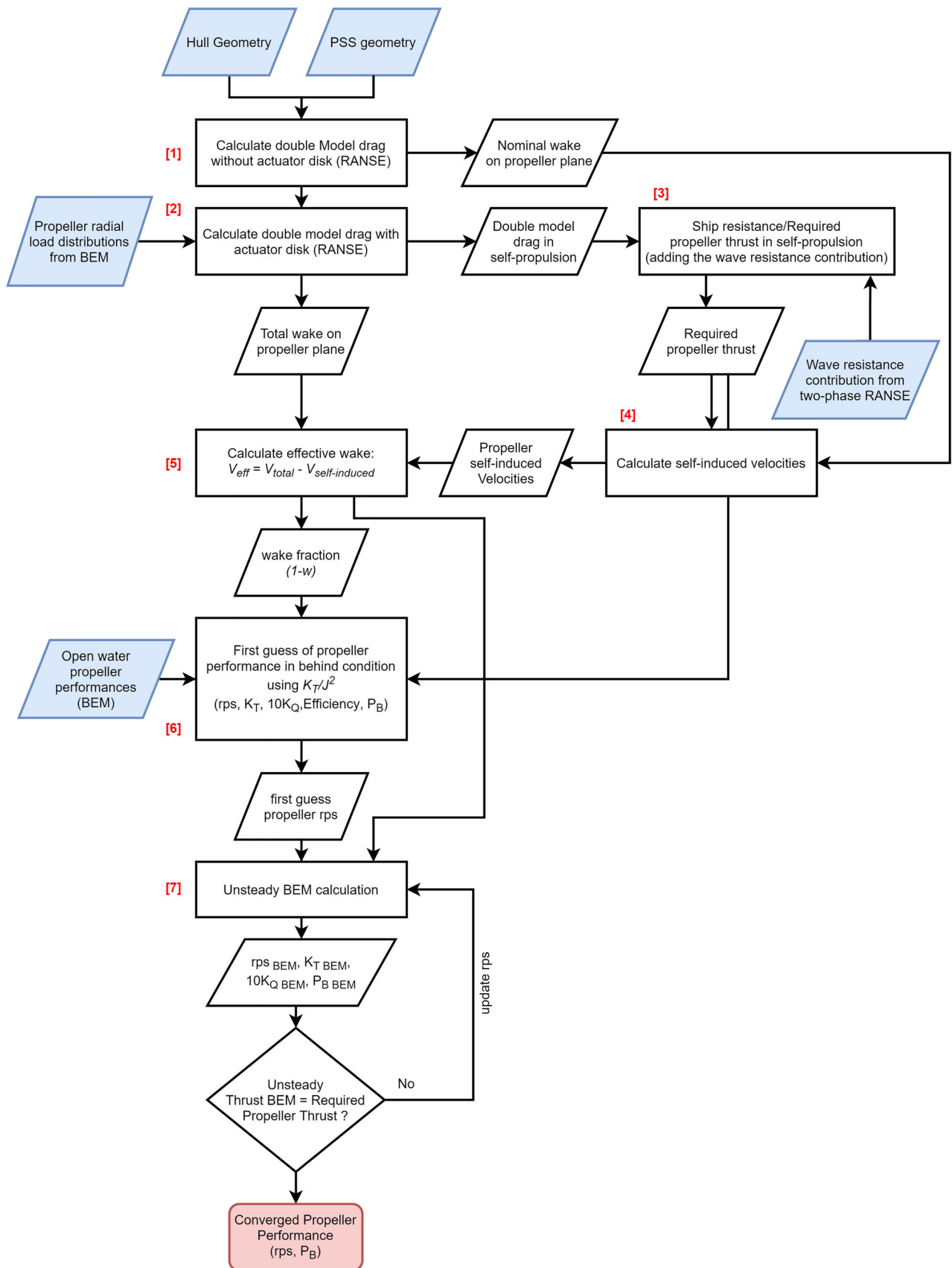
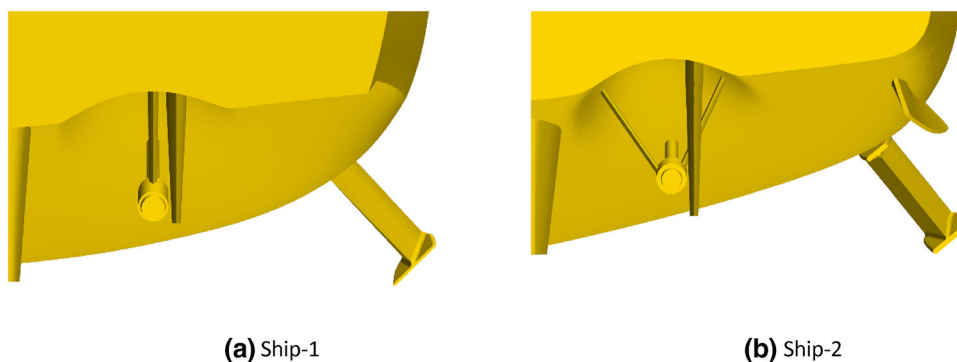


Fig. 2 Flow chart of the simplified self-propulsion evaluation process

Fig. 3 Shaft brackets arrangement for Ship-1 and Ship-2



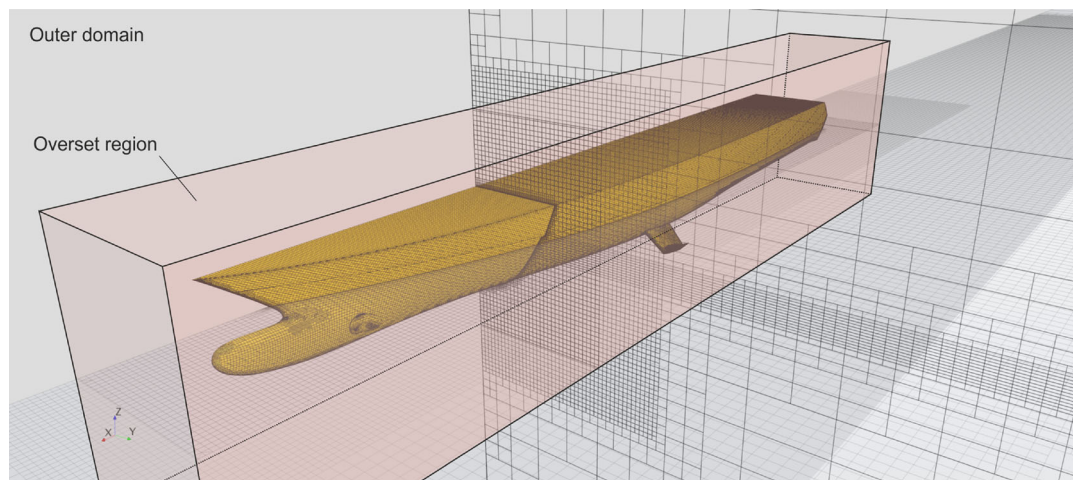
process: RANSE for ship resistance and wake prediction, BEM and RANSE for propeller performances. In absence of dedicated self-propulsion tests, fully RANSE analyses with the propeller dynamics completely resolved were employed to verify the results of the coupled approach, comparing the predicted self-propulsion points as well as the pressure distributions over the blades and the unsteady propeller thrust and torque. Self-propulsion estimations using both the methods were finally used to assess the numerical uncertainty associated with the approaches to discuss the reliability of the results and of the gains achieved by the optimized Pre-Swirl Fins. Data of Ship-2 were obtained only by numerical calculations using the mesh/panel arrangements and the numerical setups validated for Ship-1, and only a final estimation of the self-propulsion functioning, using the simplified approach and some fully RANSE analyses, is presented.

For Ship-1, at first, RANSE analyses were used to predict the ship resistance. Calculations were run in full-scale, since the ESD are designed for full-scale functioning. The validation of results is proposed, then, using the towing tank measurements appropriately scaled to ship scale. To this aim, overset meshes were employed (Fig. 4a) together with a 2-DOF two-phase flow solver with VoF capabilities. A hexa-dominant grid suitable for this type of analyses was selected based on previous calculations on similar applications using StarCCM+ (Siemens 2017). It consists (half the hull) of about 3.2 million cells organized as usual in local and anisotropic free-surface refinements needed to capture with sufficient accuracy the free surface evolution. A total of twelve (on the hull) prism layers arranged with a geometrical spacing ratio of 1.4 and for a total prism layer thickness of 120 mm, ensure a non-dimensional wall distance lower than 300 (140 in average) using the realizable $k-\varepsilon$ turbulence model. The double model, employed in the optimization activities and for deriving the “wave resistance” discussed in previous section, reduces the cells count to about 2 million (reference grid for the coupled BEM/RANSE sensitivity analyses) by avoiding the refinements in correspondence of the free surface.

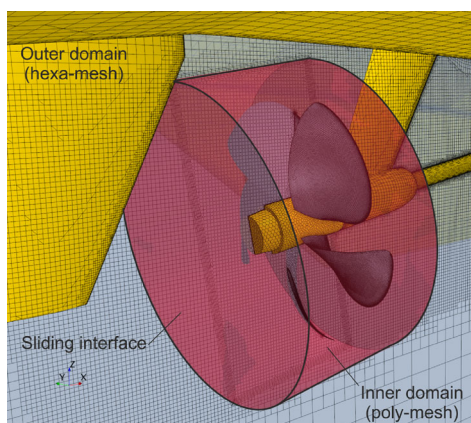
Ship performances compare reasonably well with the experimental data scaled to ship size using the ITTC’57 procedure. Ship resistance, in particular, is predicted in proximity of the design speed with an error lower than 4%, as reported in Fig. 5. Sinkage and trim show trends qualitatively in agreement with the available measurements and the differences between experimental data and computed results are in line with those observed in the case of calculations carried out for ships of comparable size and speed. The model scale nominal wake of Fig. 6 shows, too, a decent agreement compared to measurements. The decelerated flow in correspondence of the sole shaft bracket is similarly predicted in terms of magnitude and extension. The disturbance of the shaft to the inflow is well visible close to the boss cap where, unfortunately, measurements are not available. Overall, the predicted nominal wake fraction is slightly lower (about 3%) than measurements. The full-scale wake is qualitatively very similar to that computed (and measured) in model scale and only negligible differences can be observed in terms of wake fractions. Figure 7, in particular, shows a comparison between the full-scale wake computed with the double model assumption used in the optimization process and for fully resolved RANSE self-propulsion estimation and the full-scale wake computed including the free surface effect.

The computed wakes are very similar each other. The axial wake fraction using the double model assumption is 0.954, which compares very well with the wake fraction (0.957) obtained including the influence of the free surface. Qualitatively, there are only very small differences in correspondence of the shaft bracket. The in-plane component of the velocity is negligibly more oriented in the vertical direction when considering the influence of the free surface, and the shaft vortices development is slightly different. Overall, the results resemble the conclusions of Koushan et al. (2020) and Gaggero et al. (2017), allowing for reasonable predictions of the unsteady propeller performance behind the hull regardless of the inclusion of the free surface effect.

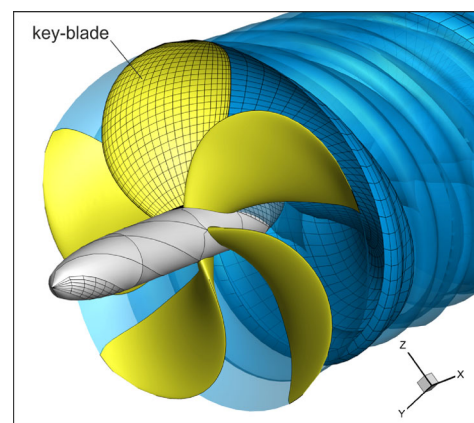
Propeller performances were evaluated using both RANSE and the Boundary Element Method. In addition



(a) Overset mesh for Ship-1 resistance and attitude prediction.



(b) Sliding mesh for RANSE self-propulsion analyses with fully resolved propeller. Ship-1



(c) BEM surface grid. Ship-1 propeller

Fig. 4 Mesh arrangement (RANSE and BEM) for ship and propeller performance prediction. **a** Overset mesh for Ship-1 resistance and attitude prediction, **b** Sliding mesh for RANSE self-propulsion analyses with fully resolved propeller. Ship-1 and **c** BEM surface grid. Ship-1 propeller

to the evaluation of the unsteady propeller characteristics required to determine the propeller delivered power (Block 7 of Fig. 2), BEM was used to identify the radial distributions of axial and tangential forces feeding the actuator disks for the approximate self-propulsion calculations. BEM analyses were carried out using the code developed at the University of Genoa, which is based on the Morino (Morino et al., 1975) formulation and on the key blade approach of Kinna and Hsin (1992) to handle the unsteadiness when the propeller operates in the wake of the ship. The reference surface mesh is that of Fig. 4c. It consists of 1250 panels per blade, solved with an equivalent time step of 6° and a steady wake alignment realized with the circumferentially averaged inflow of the nominal wake. RANSE analyses for the model scale open water calculations consider a periodic domain (one blade passage) discretized using polyhedral cells (1.2 Million) and solved in a moving reference frame. Also for

model scale analyses wall functions using the $k-\varepsilon$ turbulence model were preferred since the ten cells of the prism layers (total thickness of 1 mm) ensured a non-dimensional distance equal, in average, to 40. Results from both the codes are summarized in Fig. 8. Also in this case, the agreement between the solvers and the experimental data is good. In the operative range of $J = 0.6-0.8$ thrust is slightly underestimated (3–5% respectively for RANSE and BEM). Unexpectedly, torque is better predicted especially for RANSE (less than 1% discrepancy) while BEM calculations shows the usual limitations in heavily loaded conditions.

Fully RANSE analyses of the self-propulsion functioning were finally run mainly for validation purposes since no experimental measurements in self-propulsion are available for this ship. High-fidelity RANSE calculations including the complete dynamic of the propeller were, then, considered as reference for assessing the reliability of the coupled

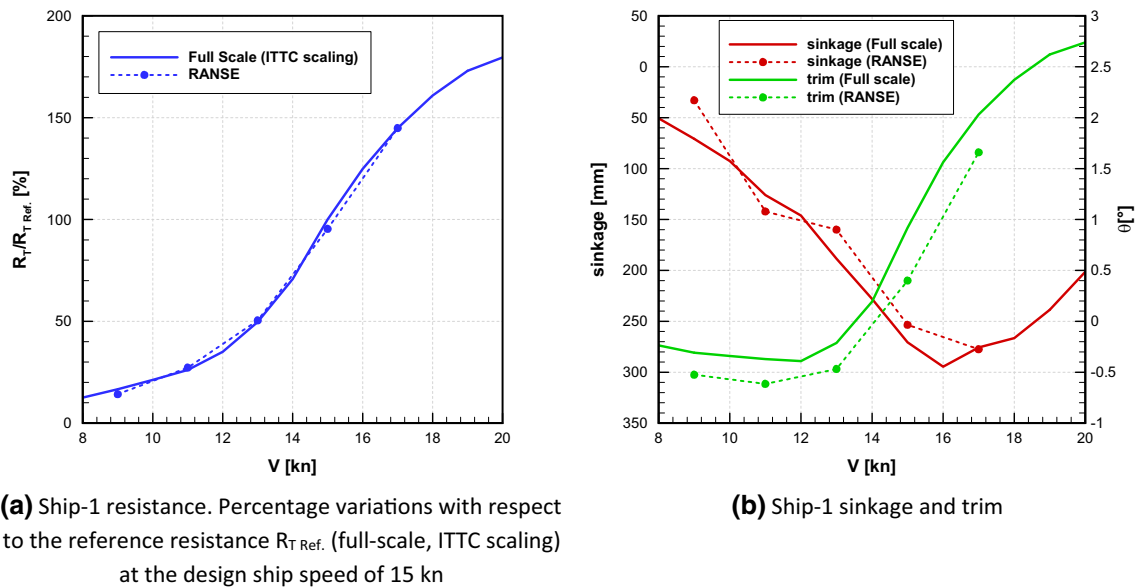


Fig. 5 Predicted ship resistance and attitude. Full-scale RANSE calculations compared to measurements (ITTC scaling), Ship-1. **a** Ship-1 resistance. Percentage variations with respect to the reference resistance $R_{T,Ref}$. (full-scale, ITTC scaling) at the design ship speed of 15 kn and **b** Ship-1 sinkage and trim

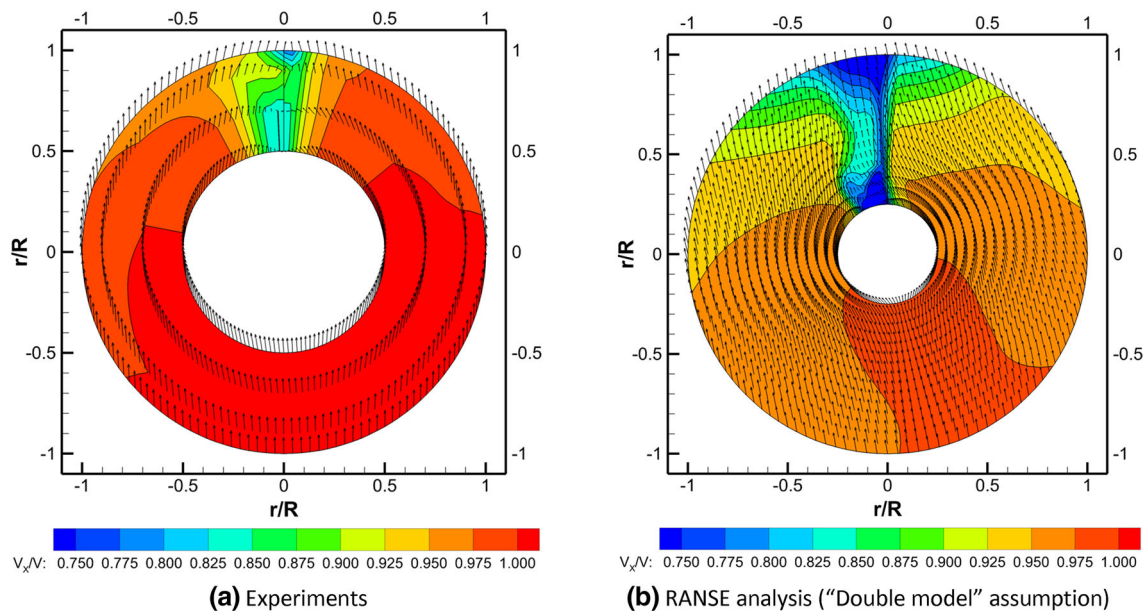


Fig. 6 Comparison between measured and computed hull nominal wake (model scale). Starboard side seen from aft, Ship-1. **a** Experiments and **b** RANSE analysis ("Double model" assumption)

procedure the optimization design method is based on. In addition, these fully RANSE calculations of the ship without the ESD represent the numerical baseline reference for estimating the savings granted by the ESDs designs at the end of the optimization activity. Again, only double model analyses, corrected with the "wave resistance" concept, were carried out using the sliding meshes of Fig. 4b. The outer domain mesh exactly resembles the arrangement devised for

the ship resistance calculations, with only the addition of few refinements in correspondence of the propeller slipstream. The inner, rotating, domain, instead, consists of polyhedral cells, which were preferred to easily handle the complexity of the flow in the surrounding of the blades as in the case of the open water analyses. Identical grid parameters, scaled to full size were consequently used, ensuring a non-dimensional wall distance in average equal to 55 with a total

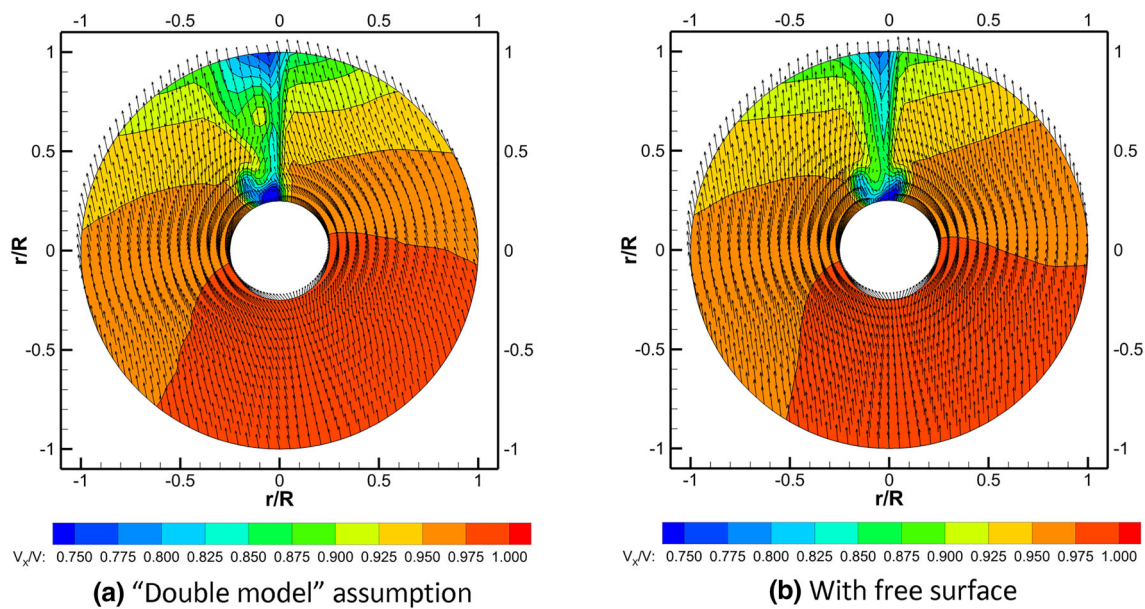


Fig. 7 Comparison between full scale nominal wakes compute with **a** the "double model" assumption and with **b** the free surface effect. Starboard side seen from aft, Ship-1

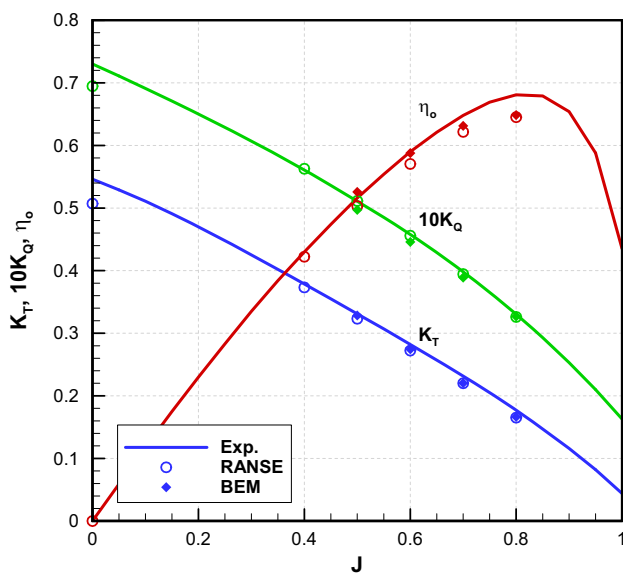


Fig. 8 Open water propeller performance prediction using BEM and RANSE, Ship-1 propeller

prism layer thickness of 3 mm. This configuration adds about 3 million cells (those of the rotating region) to the double model simulation with the actuator disk, for a total of about 5 million elements (the reference grid for fully RANSE sensitivity analyses) computed with a transient solver and a time step equivalent to 1° of propeller rotation.

The agreement between calculations, listed in Table 1, is very satisfactory. The simplified BEM/RANSE coupled method predicts the propeller rate of revolution very simi-

larly compared to the fully RANSE analyses. The difference between the delivered powers is slightly higher (about 6%), mainly as a consequence of a different prediction of the absorbed propeller torque in unsteady functioning (unsteady averaged value of 0.381 using the BEM versus 0.413 using the RANSE). Fully RANSE analyses, indeed, provide useful data to assess the reliability of the BEM calculations used in the optimization process. Among these information, unsteady propeller performances (Fig. 9) and blade pressure distributions (Fig. 10) are the most useful.

Unsteady calculations of Fig. 9 show similar trends and differences between the methods: propeller performances by RANSE are slightly higher (especially torque) than BEM, resembling what already observed in open water. Since the comparison is made between the fully RANSE analyses (i.e., propeller behind the hull, self-propulsion condition estimated using fully RANSE analyses) and the unsteady BEM using the effective wake and the propeller rate of revolution from the simplified self-propulsion estimation, this indirectly confirms the reliability of the approximated method for estimating the effective wake and the functioning point of the propeller. Also unsteady pressure distributions over the propeller blades (Fig. 10), snapshotted at several angular positions of the key blade, confirm the overall agreement between RANSE and BEM calculations. The most important features associated to the unsteady functioning of the propeller are captured by both the methods in a very similar way. Blade loading in the 50° – 180° range due to tangential velocities is observed as well as the unloading in correspondence of the 270° position, providing an indirect validation

of the pressures sampled during the optimization process to account for the risk of cavitation inception due to the pre-swirl stators modified wakes.

Starting from these reference grids configurations, the convergence trends (Eça and Hoekstra 2014) of the self-propulsion estimation (reference ship without any ESD), using both the proposed coupled BEM/RANSE and the fully RANSE approaches were investigated to verify the numerical uncertainty associated to this type of methods/calculations and the appropriateness of these reference grids for the optimization process and the final fully RANSE verification of the optimal geometries. To this aim four additional grids were derived simply by scaling the reference size of the initial configuration. In the case of the coupled BEM/RANSE approach this led to grids from 700 thousand to 5.5 million cells. In the case of fully RANSE analyses, the presence of the propeller and its local refinements produced meshes, using the same coarsening/refining rules, from 1.8 to 15.6 million elements. Results of the verification, in terms of trends of delivered power and propeller rate of revolution, are summarized in Fig. 11. It is worth to note that in these sensitivity analyses the “wave resistance”, obtained by comparing the free surface and the double model results using the reference mesh, has been maintained constant (i.e., free surface calculations have not been repeated with finer and/or coarser meshes) for any choice of the double model grid employed in the verification process. Similarly, the propeller unsteady performances using BEM in the coupled approach were always obtained with the reference surface grid of 1250 panels.

The grid convergence trend is satisfactory, especially for the coupled BEM/RANSE method that combines very different tools. When using the coupled BEM/RANSE, the

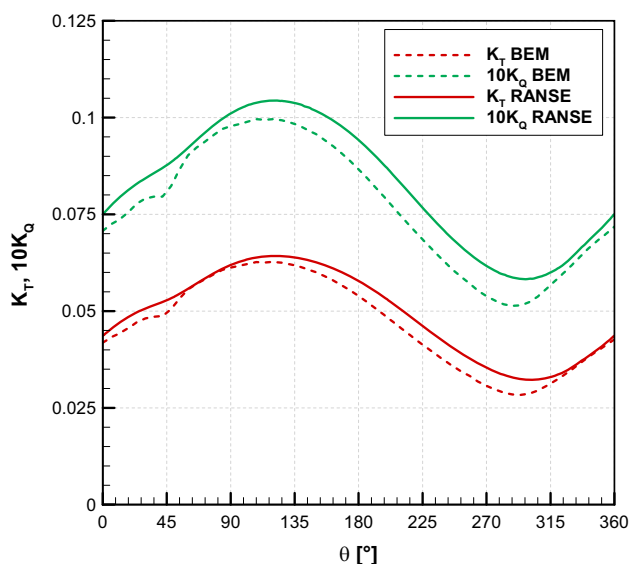


Fig. 9 Unsteady propeller performances prediction (self-propulsion condition, key blade) using BEM and RANSE, Ship-1 propeller

reference mesh provides differences, with respect to the extrapolated values, of 0.2% and 0.8% respectively for the propeller rps and the delivered power, associated to uncertainties of 0.5 and 2.3%. Similar results are confirmed by the fully RANSE analyses. In this case the overestimation of both delivered power and propeller rate of revolution of the reference mesh compared to the extrapolated value is 0.2% and 2.3% respectively. Related uncertainties are lower than 1% (0.9%) for the rate of revolution, and lower than 3% (2.8%) for the delivered power. Also the iterative convergence, monitored in Fig. 12 using the double model resistance and the single blade propeller performances, respectively for the coupled BEM/RANSE and the fully RANSE analyses, is satisfactory. Results, in this case, are shown for the reference grid. The double model resistance, after an initial transient, rapidly converges: 800 iterations are sufficient to collect data for the towing condition (averaged over the last 100), 1500 for the self-propulsion functioning using the actuator disk. Unsteady propeller performances demonstrate the iterative convergence of fully RANSE analyses. After the initialization of the calculations using steady data from a moving reference frame analysis, each step of the iterative adjustment of the propeller rps to achieve the self-propulsion functioning (thrust/resistance equilibrium) was run for ten propeller revolutions. Looking at the achieved periodic nature of the propeller performance, this seems sufficient to collect reliable time averaged data for thrust and delivered power estimations. In the light of these results, and based on the not significantly lower levels of numerical uncertainties granted by significantly denser (and computationally demanding) meshes, the reference configuration seems a good choice for the optimization-based design and for all the comparisons between the coupled BEM/RANSE and the fully RANSE calculations.

For the second ships, results of Table 2, limited only to the prediction of the self-propulsion functioning since no data are available for the validation of propeller and hull performances, mainly confirms the outcomes discussed for Ship-1 when using an identical simulation setup. In this case, the propeller computed using the BEM delivers a slightly higher thrust. For the self-propulsion functioning using the coupled BEM/RANSE this means that a reduced rate of revolution is needed and, consequently, at almost identical torque coefficient, a lower delivered power is predicted. Differences, in any case, are similar to those observed for Ship-1 and easily ascribable to the substantial simplifications accepted to realize a computationally efficient process. As extensively discussed in Furcas and Gaggero (2021), some discrepancies can be ascribed to differently computed propeller performances using the BEM especially in highly non-uniform wakes (Gaggero et al. 2014, 2019), to a different interaction of the actuator disk/fully resolved propeller with the hull and to different ways of calculating the effective wake. For the

Table 1 Self-propulsion coefficients from coupled BEM/RANSE and fully RANSE analyses at the design ship speed for the reference Ship-1 without any Pre-Swirl Stator

	Rps/rps _{Ref.} [%]	(1-t)	(1-w)	K_T	10 K_Q	η_o	$P_D/P_{D\text{Ref.}}$ [%]
Coupled BEM/RANSE	99.9%	0.947	0.930	0.231	0.381	0.636	94.4%
Fully RANSE	100%	0.933	0.932	0.240	0.413	0.612	100%

Propeller rps and delivered shaft power of coupled BEM/RANSE in percentage of reference values (rps_{Ref.} and $P_{D\text{Ref.}}$) computed using fully RANSE analyses

Table 2 Self-propulsion coefficients from coupled BEM/RANSE and fully RANSE analyses at the design ship speed for the reference Ship-2 without any Pre-Swirl Stator

	Rps/rps _{Ref.} [%]	(1-t)	(1-w)	K_T	10 K_Q	η_o	$P_D/P_{D\text{Ref.}}$ [%]
Coupled BEM/RANSE	97.0%	0.937	0.958	0.185	0.322	0.712	93.9%
Fully RANSE	100%	0.916	0.979	0.177	0.312	0.698	100%

Propeller rps and delivered shaft power of coupled BEM/RANSE in percentage of reference values (rps_{Ref.} and $P_{D\text{Ref.}}$) computed using fully RANSE analyses

latter, in particular, it is worth to note that while the coupled BEM/RANSE method computes the effective wake as the average of the local velocity field resulting from Eq. (1) (or Block 5 of Fig. 2), fully RANSE analyses rely, as in the case of towing tank measurements, to the open water propeller performances equivalence. In the case of very uneven behaviour of the port/starboard tangential flow, as the result for instance of the action of the pre-swirling fins, this could lead to very different values of wake fraction and consequently of estimated propeller efficiency. The propeller/hull interaction predicted by the coupled BEM/RANSE, moreover, is weaker (in both cases the thrust deduction factor is lower), as usually observed in literature (Starke and Bosschers 2012) when using actuator disk models, contributing to the underprediction of the shaft power. As a whole, however, these results seem more than acceptable for legitimizing

the use of the simplified self-propulsion procedure into the optimization loop.

4 Results and discussion

4.1 Reference Ship-1

Any design process based on a SBDO approach is built upon a parametric description of the geometry and an automatic “try-and-error” process using appropriate algorithms like genetic or gradient ones to realize (Pareto) convergence towards design objectives and constraints. Current pre-swirl stators have been designed following this paradigm, then starting from a parametric description of the device. Of course, a method capable of enlarging the design space as much as possible, allowing for local variations of the geometry com-

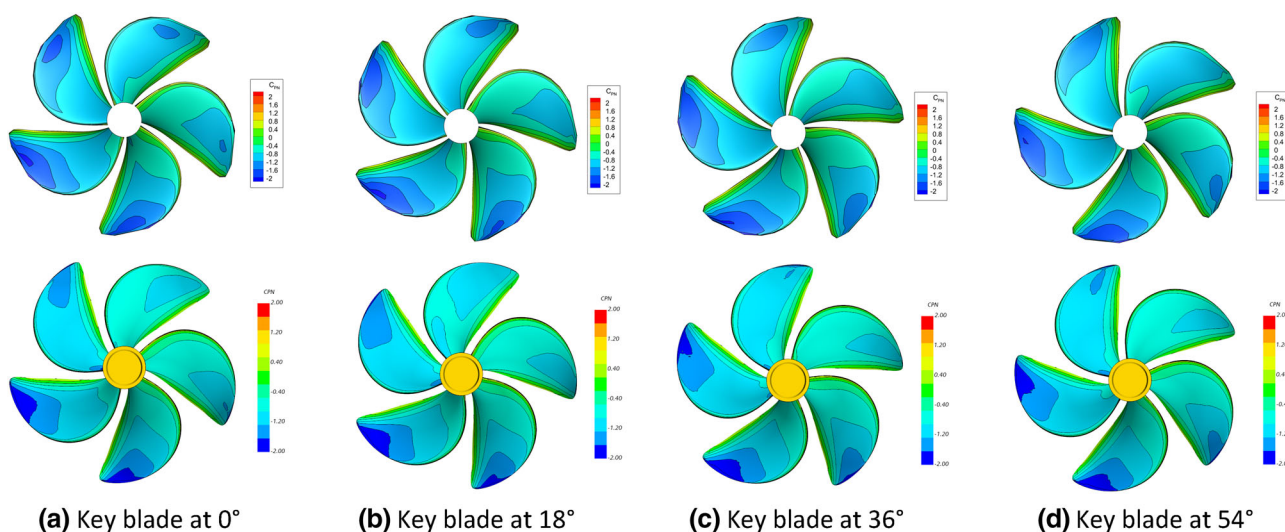


Fig. 10 Unsteady pressure distribution (C_{pN}) on the blade suction side. BEM (top) and RANSE (bottom), Ship-1 propeller in self-propulsion condition. **a** Key blade at 0°, **b** Key blade at 18°, **c** Key blade at 36° and **d** Key blade at 54°

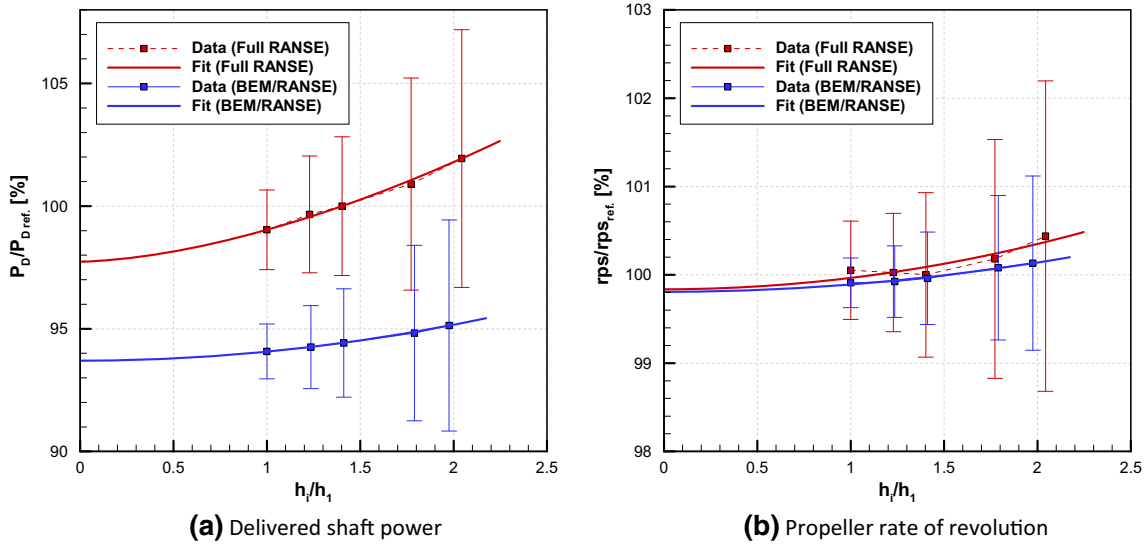


Fig. 11 Grid sensitivity analysis. Delivered shaft power and propeller rate of revolution as a function of the relative stepsize $h_i/h_1 = \sqrt[3]{n_{cells_1}/n_{cells_i}}$ where “1” is the index of the finest grid. **a** Delivered shaft power and **b** Propeller rate of revolution

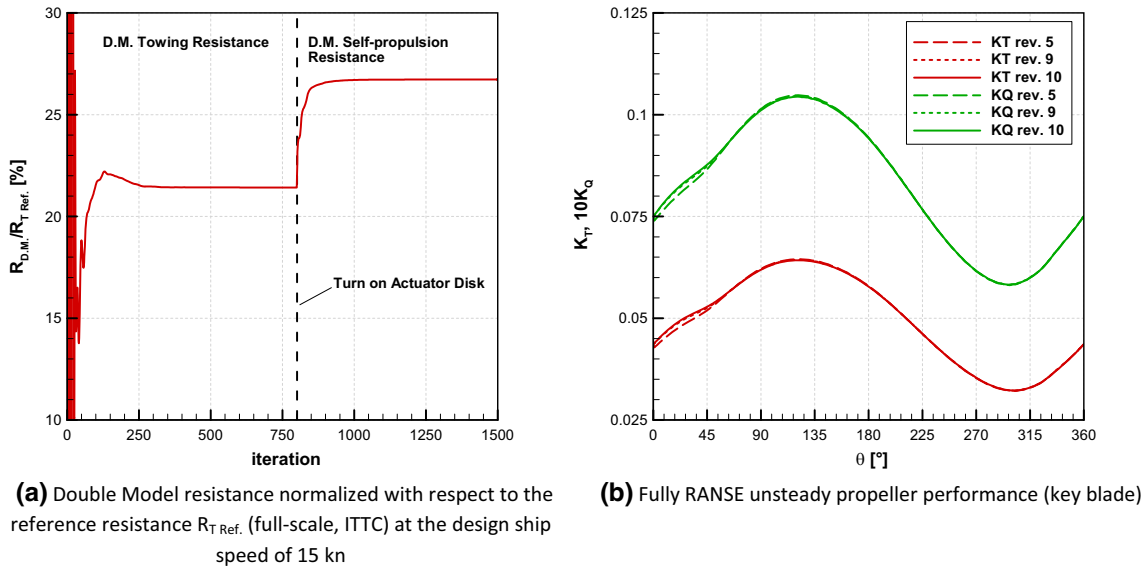


Fig. 12 Iterative convergence of the solution. **a** Double Model resistance normalized with respect to the reference resistance $R_{T.ref.}$ (full-scale, ITTC) at the design ship speed of 15 kn and **b** Fully RANSE unsteady propeller performance (key blade)

patible with the local features of the flow with the minimum possible number of design parameters would be preferable. To this aim, each fin of the pre-swirl stator was described with a linear variation of the angle of attack based on the values at root and tip, a NACA 4-digit sectional hydrofoil (maximum thickness, camber and position), a spanwise constant value of chord (equal for both the fins) and the diameter of the device (Fig. 13). With respect to the propeller, the positioning of the fins is handled by the distance from the propeller plane and by their angular location around the shaft, for a total number of design parameters equal to 14 (Table 3). The reduction of the delivered shaft power is the objective of this design case

since it summarize the effectiveness of this device as a compromise between the additional resistance of the fins and the positive influence on the propeller functioning. However, the application to a mega yacht requires attention to the propeller functioning, and in particular to a possible increased risk of cavitation (i.e., worsening of radiated noise/vibrations) as a consequence of the modification of the effective wake to the propeller. The unsteady calculations of the propeller functioning, introduced in the optimization workflow, permit the monitoring of the pressure distribution on the propeller blades, which can be easily translated into a new set of design objectives dealing with the risk of cavitation. Then, the final

Table 3 Ranges of design parameters and geometry of the optimized pre-swirl devices. Ship-1

Design parameter		Min	Max	Pre-4491
Pre-swirl diameter/propeller diameter	P1	0.85	1.25	1.08
Fins chord (same for both)	P2	0.15 m	0.30 m	0.22 m
Max camber/Chord (first fin)	P3	− 0.05	0.05	− 0.002
Max camber/Chord (second fin)	P4	− 0.05	0.05	− 0.047
Max thickness/Chord (same for both)	P5	0.075	0.15	0.125
Position of max camber/chord (first fin)	P6	0.3	0.6	0.4
Position of max camber/chord (second fin)	P7	0.3	0.6	0.6
α at root (first fin)	P8	− 17.5°	17.5°	− 0.5
α at tip (first fin)	P9	− 17.5°	17.5°	0.5
α at root (second fin)	P10	− 17.5°	17.5°	11.5
α at tip (second fin)	P11	− 17.5°	17.5°	− 9.5
θ_1	P12	0°	230°	220
θ_2 /remaining angular space	P13	0	1	0.28
DX/hub length	P14	0	1	0.11

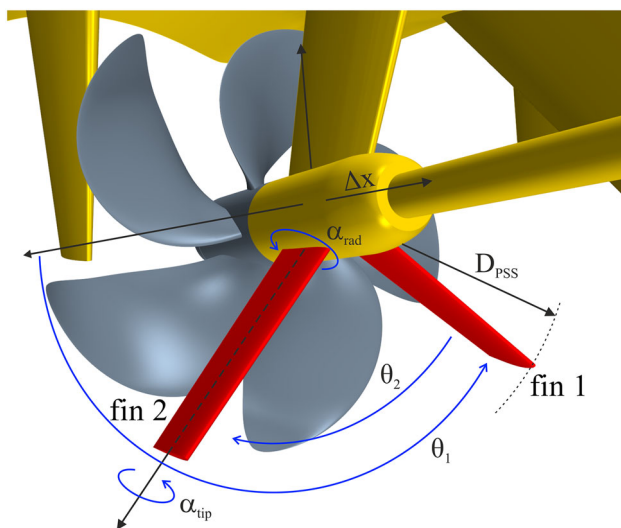


Fig. 13 Parametric description of the pre-swirl fins. Shaft arrangement of Ship-1

process accounts even for the risk of cavitation by collecting the maximum value of suction (i.e., the computed inception index) on the back of the blade during a complete revolution (for the reference case: $-C_{PN Max}$ equal to 2.08 using the coupled BEM/RANSE). Besides, the average value of the pressure coefficient (for the reference case: $-C_{PN Avg}$ equal to 1.68), which in some way gives an idea of the extent of the flow disturbance induced by the fins, is gathered as well. For this analysis, a multi-objective optimization algorithm (also in this case of genetic type) is mandatory. The design space was filled with 140 initial configurations (Latin Hypercube Sampling) and a total of 2800 cases (20 times the initial population) have been derived using the modeFRONTIER optimization environment (Esteco 2017). The results of the

optimization activity are summarized in the Pareto diagram of Fig. 14 while the influence of the design parameters on the design objectives is highlighted by some statistical indexes (*t* test) in Fig. 15. In addition to all the possible optimal configurations on the Pareto front, indeed, with the aid of a *Student test* it is possible to derive the strength of the relationship between the input design parameters and the outputs. Since the sampling of the design space was not properly distributed, being the result of an optimization activity which subsequently clustered points around the Pareto front, this test cannot be considered conclusive but can serve as a general design guidelines highlighting useful trends. The sign, besides, provides an indication circa the kind of the rela-

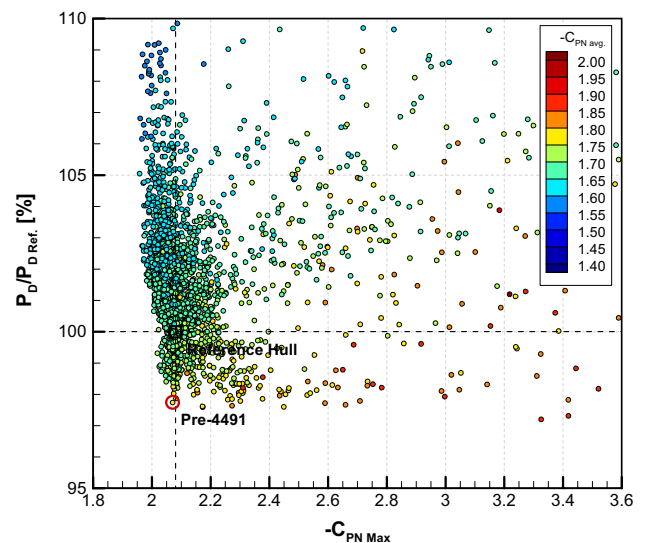


Fig. 14 Pareto-convergence of the Pre-Swirl fins optimization process, Ship-1. Delivered power non-dimensional with respect to that delivered power (BEM/RANSE coupling) of the reference Ship-1

tionship, direct or inverse, among inputs and outputs. For delivered power reduction, the second fin seem to be the most influential since parameters 11 (tip angle of the second fin) and 4 (maximum camber of second fin) have some of the highest normalized effect. The position of the fins (parameters 12 and 13, respectively for the first and the second) is as much important. This analysis suggests a positioning of the fins on the port side, as close as possible to the vertical position (i.e. to the shaft bracket), in a way similar to that observed in the case of fully blocked ships analyzed in Furcas and Gaggero (2021), Koushan et al. (2020), Kim et al. (2013). Other parameters, as for instance those that describe locally the fins sectional hydrofoil shape, instead seems less important.

The effectiveness of the pre-swirling action of the device, within the limitations of the approximated self-propulsion estimation method, is clear already by the simplified analyses using the coupled BEM/RANSE carried out in the optimization process. As usual when dealing with contrasting objectives, the highest reduction of absorbed power corresponds to the cases where the risk of cavitation is higher. Luckily, there are also several geometries capable of ensuring a simultaneous reduction of both the design objective. Among these, Pre-4491 is the configuration that realizes the maximum reduction of delivered power at a slightly lower risk of cavitation. Based on this, it has been chosen as the optimized configuration to be further analyzed using full RANSE calculations to investigate also the off-design functioning of the energy saving device.

Complete full RANSE analyses confirm the reductions of delivered power observed in the optimization process, predicting a saving of about 2.9% (Table 4). Fully RANSE analyses of this final configuration highlight once more the limitations of the BEM/RANSE calculations already discussed for the reference ship without PSS, but support the trends evidenced by the simplified calculations during the optimization. As for the reference case, the coupled BEM/RANSE approach underestimates the hull/propeller interaction, which is on average 1% higher when computed with the fully resolved propeller. Delivered thrust and absorbed torque by the propeller reflect this discrepancy that is further intensified by the limitations of BEM in dealing with strongly non-homogeneous inflow wakes, as those from the pre-swirl stators. The most significant difference between the two approaches can be observed, however, in the predicted effective wake fractions (those from the BEM/RANSE coupled method are collected in Fig. 16) and, consequently, in the predicted propeller efficiency.

As discussed in similar analyses (Furcas and Gaggero 2021) the reduction of the wake fraction up to 7–8% (fully resolved propeller) compared to the marginal reductions observed using the simplified BEM/RANSE approach in presence of the pre-swirl stators is due to the different way

the effective wake fraction is computed. Using the coupled BEM/RANSE method, the estimation of the wake fraction is carried out directly through an average over the effective wake (which is calculated by the coupling algorithm) on the propeller disk. On the other hand, fully RANSE analyses exploit the open water propeller diagram and the information from the self-propulsion calculations (propeller delivered thrust and rate of revolution) to assess the wake fraction required to meet the thrust identity between the thrust coefficient delivered in open water conditions and that delivered behind the hull. Regardless a certain difference between these two ways of calculating the wake fraction (i.e., body forces tendency to underestimate the flow deceleration), however, the port/starboard non-symmetrical tangential components of the flow to the propeller caused by the pre-swirl fins have to be considered. Tangential flow contributes to the blade delivered thrust increase by changing the local angle of attack without any change in the axial flow that, instead, is the only parameter responsible for the thrust identity when the usual definition of wake fraction based on equivalent open water propeller performance is adopted. This causes an over-estimation of the wake fraction/flow deceleration when its calculation is based on the thrust identity assumption (as in the case of fully resolved RANSE analyses). The effect of the port/starboard uneven tangential flow in increasing the propeller delivered thrust is not considered and it is consequently balanced by a false deceleration of the axial wake. On the contrary, the wake fraction computed by averaging the effective wake accounts only for the current local axial velocity (and not of the influence on the thrust of the tangential flow), resulting in a significantly faster average inflow. The calculation of the propeller efficiency, which is strictly correlated to the wake, appears to depend on these differences. Since the operative point of the propeller significantly moves towards lower advance coefficients, the propeller efficiency predicted using fully resolved RANSE analyses is reduced, but it is largely compensated by a significant increase of the hull efficiency (not observable in the case of BEM/RANSE coupled analyses) that implicitly accounts for the different calculation methods.

Figure 17 compares the unsteady propeller performances (thrust coefficient, key blade, using the fully RANSE and the coupled BEM/RANSE) in presence of the Pre-4491 with the reference geometry. The agreement between coupled BEM/RANSE and fully RANSE analyses is good, regardless the apparent differences in the wake fraction (that are fully compensated in the real flow including radial and tangential components) confirming that differences observed in Table 4 are the results only of a difference the way the wake fractions are calculated.

The deviation between the methods is comparable to that already discussed for the reference ship without PSS (Fig. 9) but in both cases and especially when considering the pro-

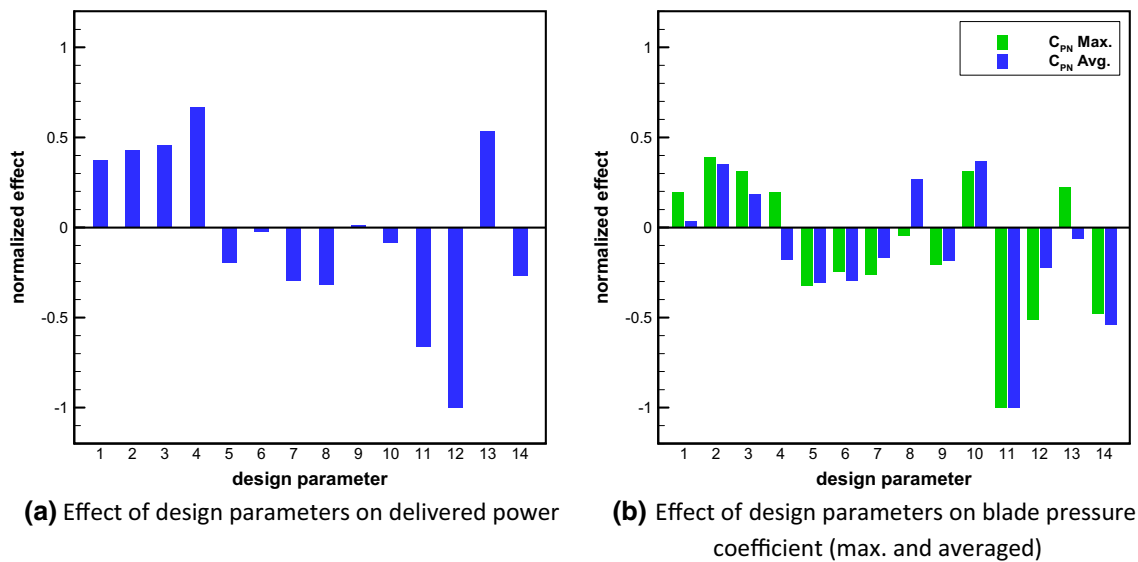


Fig. 15 t-Student tests and effect size of the design parameters on design objectives, Ship-1. **a** Effect of design parameters on delivered power and **b** Effect of design parameters on blade pressure coefficient (max. and averaged)

Table 4 Self-propulsion coefficients from coupled BEM/RANSE and fully RANSE analyses at the design ship speed for the optimal Pre-Swirl configurations, Ship-1

	rps/rps _{Ref.} [%]	(1-t)	(1-w)	K_T	10 K_Q	η_o	$P_D/P_{D\text{Ref.}}$ [%]
Ref. Ship-1, BEM/RANSE	100%	0.947	0.93	0.231	0.381	0.636	100%
Ref. Ship-1, Full RANSE	100%	0.933	0.932	0.240	0.413	0.612	100%
Pre-4491 Ship-1, BEM/RANSE	97.20%	0.948	0.929	0.247	0.408	0.656	97.80%
Pre-4491 Ship-1, Full RANSE	97.10%	0.940	0.866	0.255	0.438	0.588	97.10%

Propeller rps and delivered shaft power always in percentage of the values (rps_{Ref.} and $P_{D\text{Ref.}}$) of the reference Ship-1 computed using respectively the BEM/RANSE coupled solver and the fully RANSE analyses

propeller performances computed with the BEM, it is possible to appreciate the higher relative increase of load in the range 180°–300°, ascribable to the modification induced to the inflow wake by the pre-swirl stators.

Off-design functioning, which was tested for ship speeds of 13 and 17 kn, reveal very similar results. Calculations were carried out using full RANSE analyses only and an overview of self-propulsion coefficients is given in Fig. 18. Compared to the reference Ship-1, the presence of the optimized Pre-4491 PSS ensures a reasonable energy saving, always greater than 2%, for any ship speed under investigation, corresponding to reduction of the propeller rate of revolution close to 3% in correspondence of the lower ship speed. Wake fraction and thrust deduction convey the influence of the energy saving device similarly at any functioning and in accordance with what observed for slow, fully blocked, and ships: the thrust deduction is lower in presence of the PSS while the effective wake, again as a consequence of the open water thrust equivalence approach, is significantly slower.

Finally, the snapshots of the pressure distributions on the propeller blades of Fig. 19 confirm the influence of the pre-swirl device on the cavitation inception. Although the time histories of the pressure field were not collected during the fully resolved RANSE analyses, excluding the possibility of a direct comparison with the quantities extracted during the optimization process, from a qualitative point of view these pressure distributions are sufficient demonstrate the reliability of the design process since the angular positions of the five blades of the propeller encompass the most critical conditions (for what concern the risk of cavitation inception) of a typical inclined shaft functioning. The influence of the pre-swirl Stator is mostly evident in the second half of the propeller revolution (180°–360°) where the swirling effect and the flow deceleration provided by the pre-swirl stator efficiently combine to increase the usually low loading of the propeller blades typical of inclined shaft configurations. In the first half of the propeller revolution, the influence of the pre-swirl fins is almost negligible. Similarly to what observed using the combined BEM, also using fully resolved RANSE

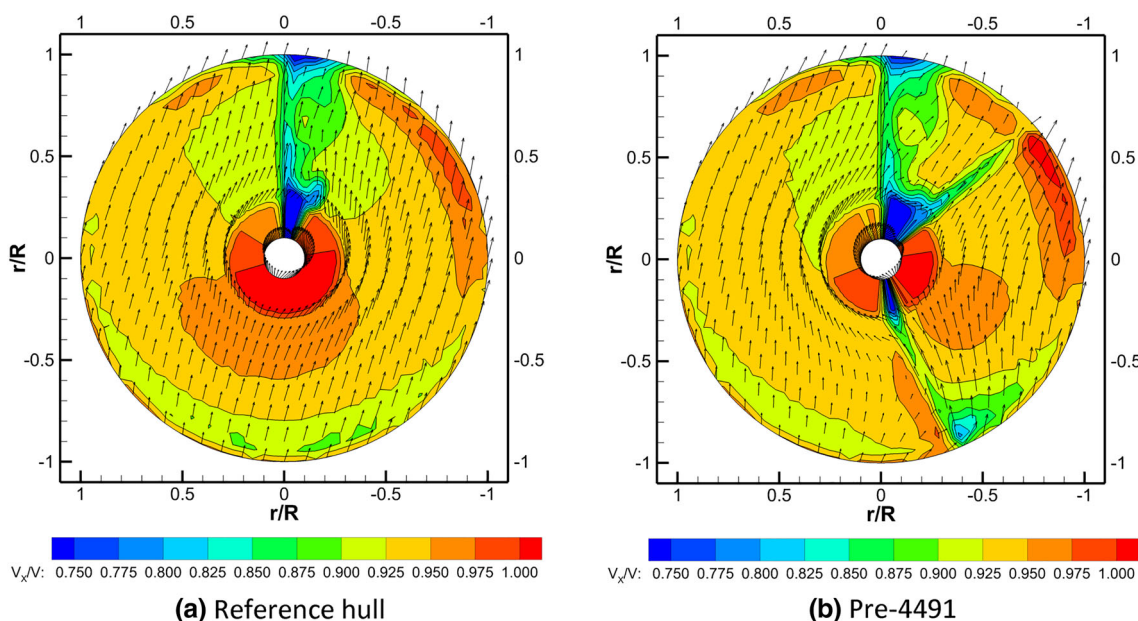


Fig. 16 Comparison of the effective wakes predicted by the coupled BEM/RANSE method. Starboard side seen from bow, Ship-1. **a** Reference hull and **b** Pre-4491

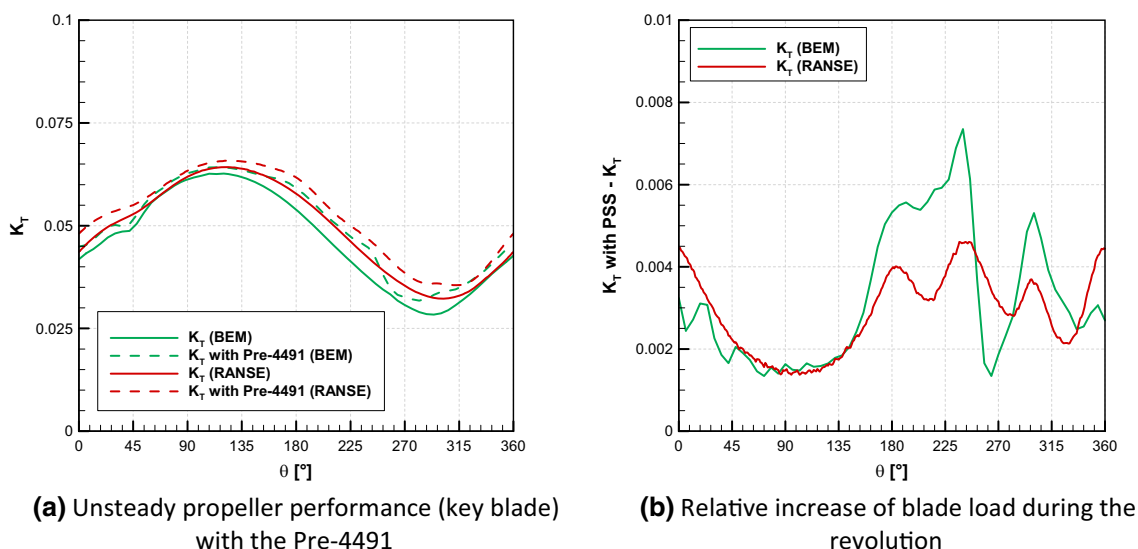


Fig. 17 Unsteady propeller performances prediction (self-propulsion condition, key blade) using BEM and RANSE, Ship-1 propeller with and without the optimal Pre-4491 Pre-Swirl Stator. **a** Unsteady propeller performance (key blade) with the Pre-4491 and **b** Relative increase of blade load during the revolution

calculations, pre-4491 results as the configuration capable of even ensuring an improvement in terms of cavitation inception, which is evident in current calculations by the reduction of suction when the blade passes through the lower portion of the disk.

4.2 Reference Ship-2

The design activity for the Pre-Swirl Stator of Ship-2 was carried following the same procedure adopted for Ship-1, then

by requiring the simultaneous minimization of the absorbed power controlling, at the same time, the risk of cavitation inception by monitoring the maximum and the average values of suction on the propeller blades collected during the analyses. Based on the results of Ship-1, and in particular having in mind the relatively low effect of some design parameters on the design objectives (Fig. 15), the parametrization of the ESD geometry was simplified by reducing their number to only ten. In particular, the position of the ESD with respect to the propeller was disregarded as well as some parameters

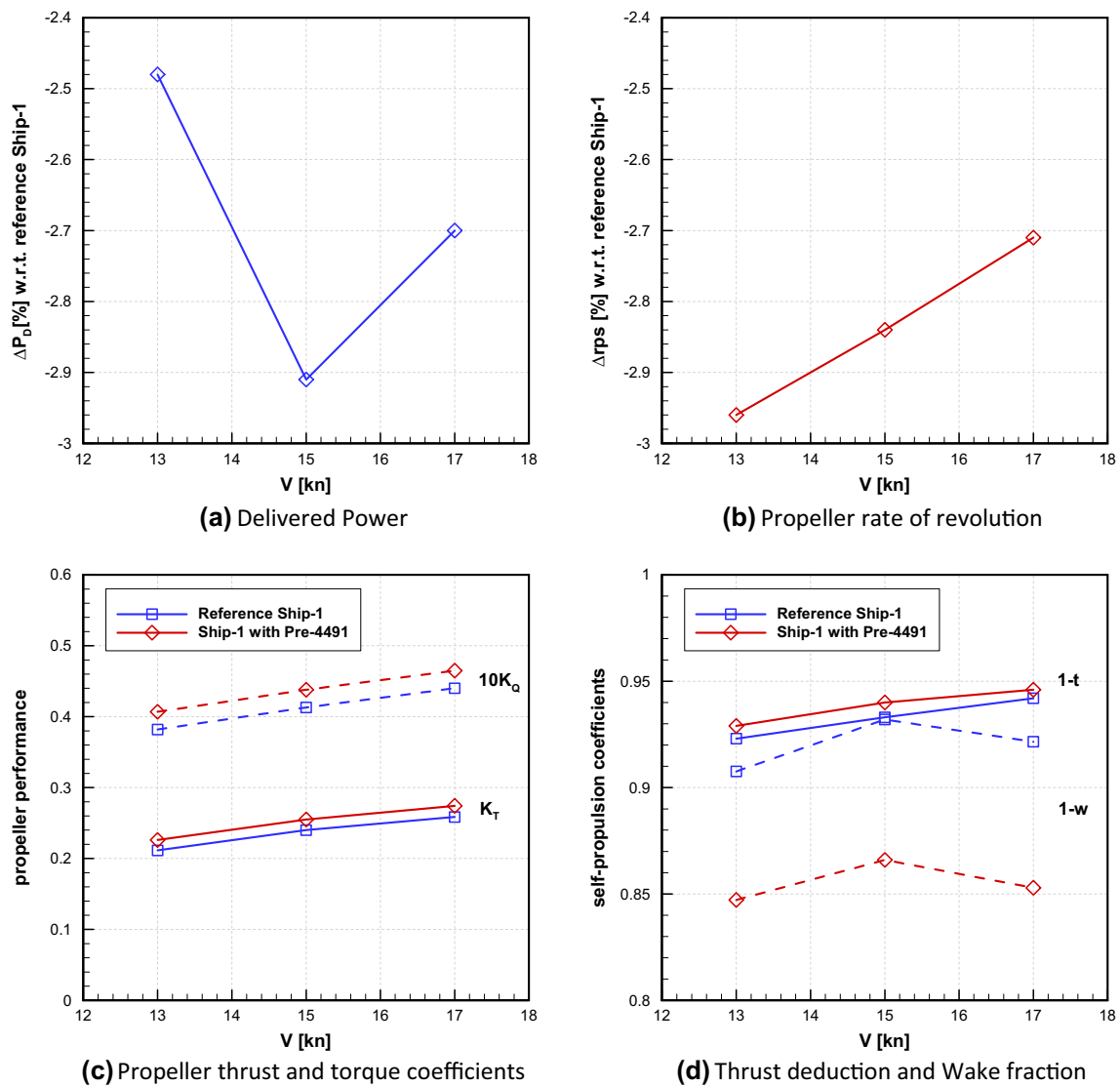


Fig. 18 Self-propulsion performances using fully RANSE analyses in off-design conditions. Propeller rps and delivered shaft power always in percentage of the values ($rps_{Ref.}$ and $P_{D,Ref.}$) of the reference Ship-1

at equivalent ship speeds. **a** Delivered power, **b** Propeller rate of revolution, **c** Propeller thrust and torque coefficients and **d** Thrust deduction and wake fraction

describing the local shape of the hydrofoil, like the position of the maximum camber and the maximum thickness, which were fixed respectively equal to $0.4 x/c$ and $0.12 t/c$. The final choice of the design parameters, with the adopted range of variation adjusted for this design, is collected in Table 5.

In the context of affordable optimization-based design procedure, the design activity for Ship-2 represents a test case for the application of surrogate modeling to the design process. Regardless the use of simplified self-propulsion estimation methods, like the coupled BEM/RANSE successfully adopted for the design of the Pre-4491 for Ship-1, the numerical estimation of the two thousand, eight hundred different configurations needed to achieve a sufficient Pareto convergence requires an amount of time not afford-

able for very preliminary design activities. This effort can be significantly reduced by the use of surrogate modeling. A surrogate model is, essentially, a response function fitted to basic data, obtained by evaluating objectives and constraints of the design in correspondence of few sampling points of the design space, through which build a meta-model of the phenomena under investigation (Forrester et al. 2008). The response function can be efficiently used, then, to gather data, correlations, tendencies and, eventually, build a new design by optimization process, as done in current design activity. The steps required for a robust surrogate definition for optimization purposes involve a sampling (1) of the design space to gather all the necessary data (objective/constraint) from an initial set of configurations, through which build (2) the

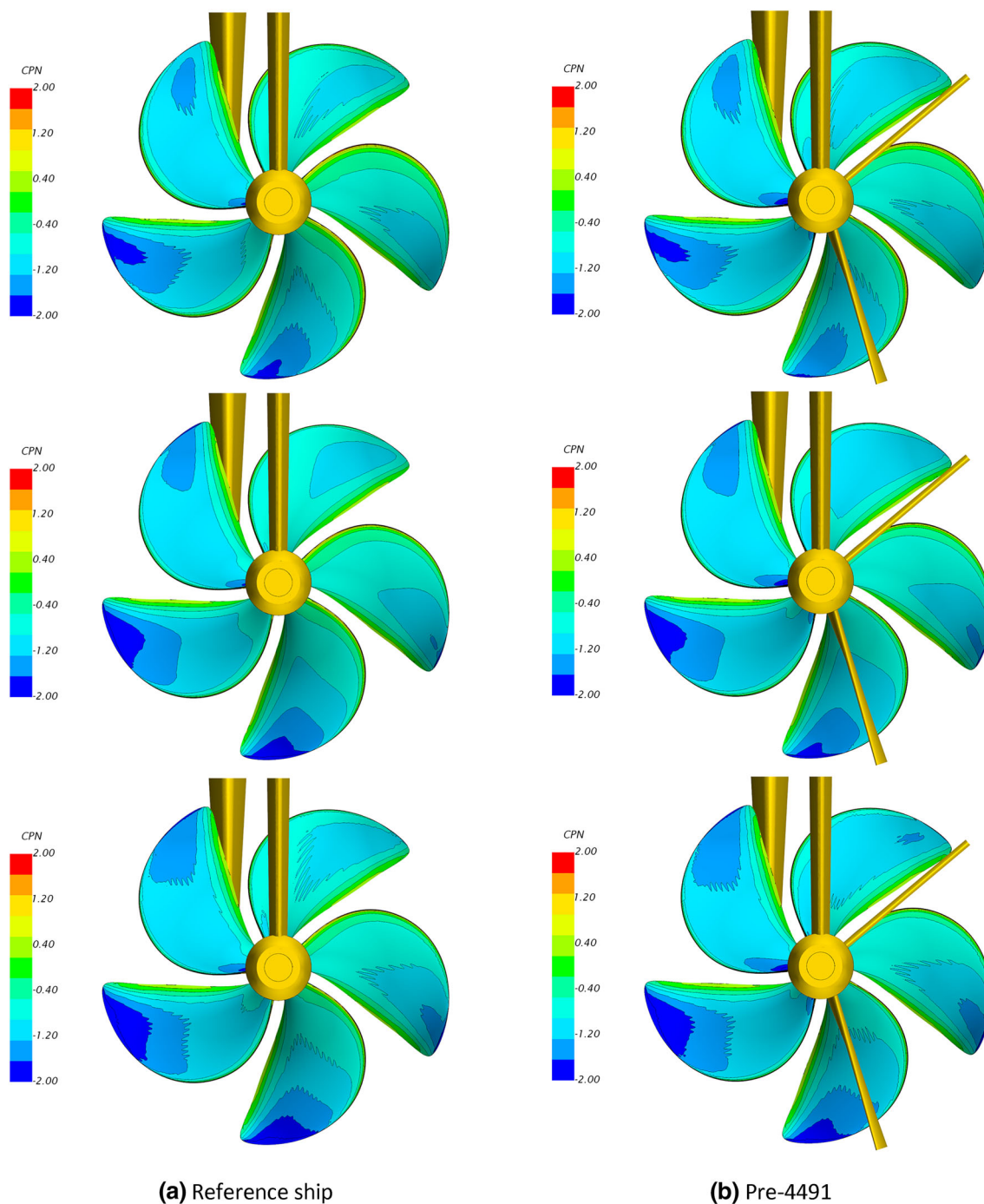


Fig. 19 Optimal Pre-Swirl fins arrangement and pressure coefficient (C_{PN}) on the starboard propeller blades, seen from bow (suction side). Comparison with the reference configuration of Ship-1. From top to bottom, ship speeds of 13, 15 and 17 kn. **a** Reference ship and **b** Pre-4491

surrogate model itself and validate it (3) identifying some characteristic statistical metrics. An update of the metamodel (4), by its “re-training” on an enlarged set of data selected on the basis of the first runs of the optimization process or of some estimation of the levels of uncertainty of the model, can finally improve its predictive capabilities.

For current design activity, surrogate models based on the Kriging approximation have been selected. In particular, the Ordinary Kriging provided by the DACE toolbox (Lophaven et al. 2002) was used to build the response surfaces of the objectives of the design (i.e. delivered propeller power and cavitation indexes using the pressure coefficients), being the

Table 5 Ranges of design parameters and geometry of the optimized Pre-Swirl devices. Ship-2

Design parameter		Min	Max	Pre-2017
Pre-swirl diameter/propeller diameter	P1	0.85	1.05	0.98
Fins chord (same for both)	P2	0.15 m	0.35 m	0.26 m
Max camber/Chord (first fin)	P3	− 0.05	0.05	− 0.017
Max camber/Chord (second fin)	P4	− 0.05	0.05	− 0.027
α at root (first fin)	P5	− 15°	15°	7.5
α at tip (first fin)	P6	− 15°	15°	4.5
α at root (second fin)	P7	− 15°	15°	− 3.5
α at tip (second fin)	P8	− 15°	15°	− 1.5
θ_1	P9	5°	160°	75
θ_2 /remaining angular space	P10	0	1	0.82

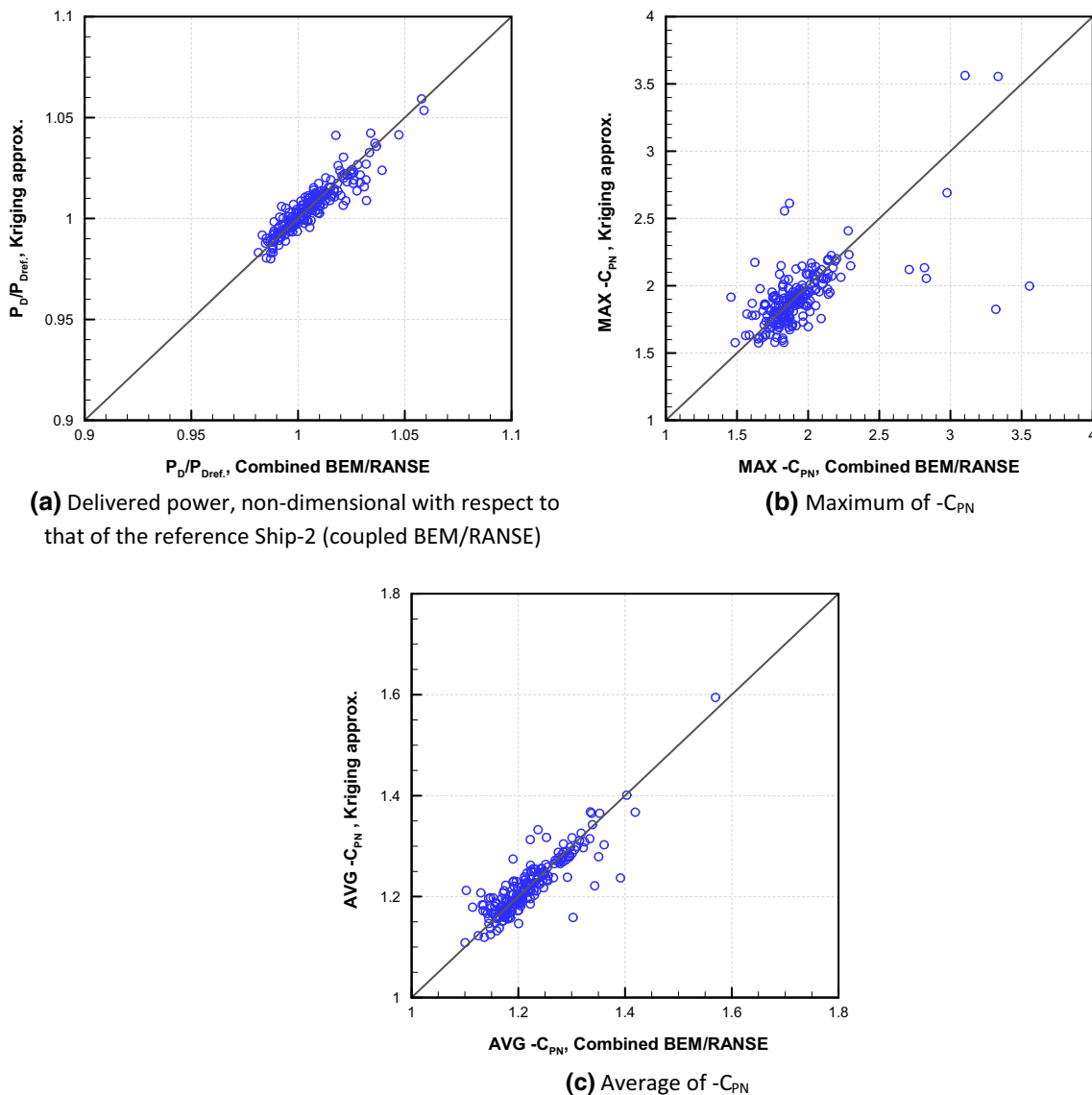


Fig. 20 Correlation diagrams between calculated (Combined BEM/RANSE) and approximated (Kriging) data. **a** Delivered power, non-dimensional with respect to that of the reference Ship-2 (coupled BEM/RANSE), **b** Maximum of $-C_{PN}$ and **c** Average of $-C_{PN}$

Table 6 Metrics of the ordinary Kriging models

Quantity of interest/design objective	Err%	Std (err%)	R^2
Delivered power	0.36%	0.37	0.854
$-C_{PN \text{ Max}}$	6.17%	7.31	0.640
$-C_{PN \text{ Avg}}$	1.60%	1.88	0.760

constraints already coded into the geometric parametrization of the system. Validation was carried out at first. Validation means, essentially, measuring the goodness of the surrogate with respect to the “true” calculations to evaluate its potential to globally approximate the design space. Once trained, the classical validation of the surrogate is carried out by sampling once more the design space, by estimating the performance of this new set of M samples using both “true” calculations and the surrogate itself and by computing a set of statistics from these data. Classical error measures are the average percentage error, its standard deviation and the coefficient of determination R^2 which, all together, provide a picture of the surrogate model approximations.

For current design case, the design space identified by range of variations of the free parameters listed in Table 5, was initially sampled using Latin Hypercube to identify 200 initial configurations which performances, computed using the coupled BEM/RANSE method, serve as training set. Additional 200 geometries were selected randomly to provide data for the validation of the metamodels using the metrics collected in Fig. 20 and Table 6.

Based on the validation results, the interpolating capabilities of the surrogate models built for any of the design objectives of the optimization process seem reasonable. For what concern the delivered power and the averaged value of the pressure coefficient, in particular, the percentage error is very small, and the coefficient of determination which provides a measure of how well observed/computed outcomes are replicated by the metamodel, is sufficiently high. The approximation of the maximum of the pressure coefficient poses some issues since the averaged error is about 6% and the correlation between approximated and computed data is not particularly high. Since the preferred result of the design is the minimization of the delivered power and the risk of cavitation is monitored mainly as a constraint in the selection of the optimal configuration (only to avoid excessively unbalanced solutions), the use of these models seems credible. Then, using the sampling devised for the training of the models, 4000 cases (again 20 times the initial population, Fig. 21) have been derived and the Pre-2017 configuration has been selected as the best design (minimum of resistance at a slightly higher value of cavitation inception) to be investigated using “true” coupled BEM-RANSE and fully RANSE analyses.

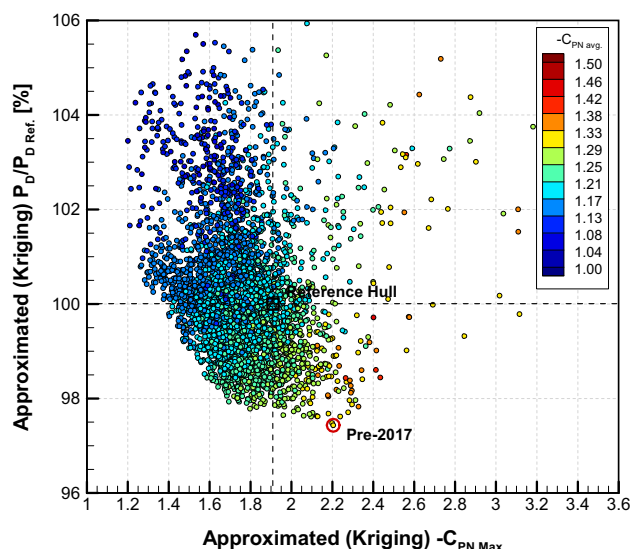


Fig. 21 Pareto-convergence using surrogate modelling of the Pre-Swirl fins optimization process, Ship-2. Delivered power non-dimensional with respect to that (BEM/RANSE coupling) of the reference Ship-2

Results of “true” calculations confirm the outcomes of the optimization process based on surrogates. Compared to the performance of the reference Ship-2 evaluated with the coupled BEM/RANSE method ($-C_{PN \text{ Max}}$ of 1.91, $-C_{PN \text{ Avg}}$ of 1.21), the surrogate models foresee for the optimal geometry a reduction of delivered power of about 2.6% and cavitation inception ($-C_{PN \text{ Max}}$ at 2.2 ($C_{PN \text{ Avg}}$ of 1.21). Calculated data using the coupled BEM/RANSE and the fully RANSE realize almost the same reduction of power (2% in average, as in Table 7) with a risk of cavitation (BEM-RANSE analyses) fixed at 2.13 ($C_{PN \text{ Max}}$) and 1.31 ($C_{PN \text{ Avg}}$).

Predicted self-propulsion coefficients behave similarly to Ship-1. The presence of the Pre-Swirl alters the wake fractions, especially in the case of the fully RANSE analyses that again calculate it through the thrust equivalence rather than by the integration of the axial velocity field on the propeller plane (Fig. 22). Also off-design functioning (Table 8), in this case for a ship speed of 17 kn, prove the effectiveness of the design, which is capable of a saving slightly higher than 2%. For both the functioning conditions, the risk of cavitation seems not worsened also when comparing fully RANSE calculations of the reference and the optimized Pre-Swirl Stator of Fig. 23, confirming the suitability of the performance indicators exploited in the design process.

5 Conclusions

In the present work, the design of energy saving devices based on the pre-swirl stator concept is illustrated using an optimization process. Thousands of different configurations are

Table 7 Self-propulsion coefficients from coupled BEM/RANSE and fully RANSE analyses at the design ship speed for the optimal Pre-Swirl configurations, Ship-2

	rps/rps _{Ref.} [%]	(1-t)	(1-w)	K_T	10 K_Q	η_o	$P_D/P_{D\text{Ref.}}$ [%]
Ref. Ship-2, BEM/RANSE	100%	0.9372	0.9579	0.185	0.3223	0.712	100%
Ref. Ship-2, Full RANSE	100%	0.916	0.979	0.1772	0.31159	0.6975	100%
Pre-2017, Ship-2, BEM/RANSE	97.7%	0.9404	0.9572	0.1944	0.338	0.7292	97.9%
Pre-2017, Ship-2, Full RANSE	98.0%	0.935	0.9428	0.1847	0.32399	0.6868	98.1%

Propeller rps and delivered shaft power always in percentage of the values (rps_{Ref.} and P_{D Ref.}) of the reference Ship-2 computed using respectively the BEM/RANSE coupled solver and the fully RANSE analyses

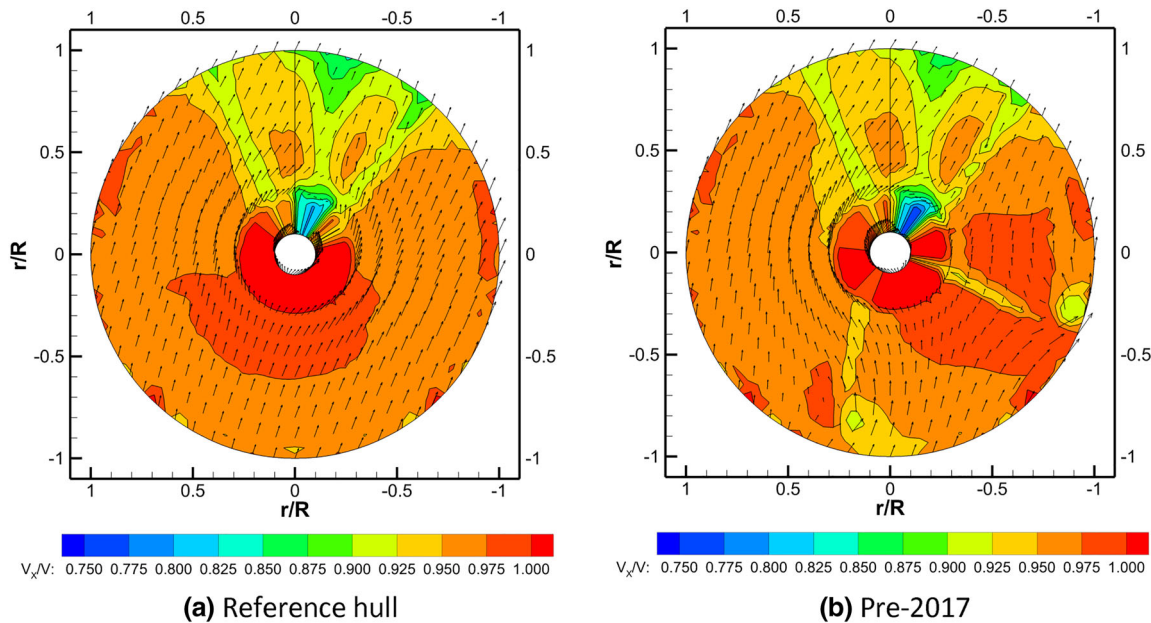


Fig. 22 Comparison of the effective wakes predicted by the coupled BEM/RANSE method. Starboard side seen from bow, Ship-2, **a** Reference hull and **b** Pre-2017

Table 8 Off-design (17 kn) self-propulsion coefficients from coupled BEM/RANSE and fully RANSE analyses for the optimal Pre-Swirl configurations, Ship-2

	rps/rps _{Ref.} [%]	(1-t)	(1-w)	K_T	10 K_Q	η_o	$P_D/P_{D\text{Ref.}}$ [%]
Ref. Ship-2, Full RANSE	100%	0.912	0.951	0.2163	0.3628	0.6631	100%
Pre-2017, Ship-2, Full RANSE	98.0%	0.921	0.9099	0.2248	0.3764	0.6493	97.7%

Propeller rps and delivered shaft power always in percentage of the values (rps_{Ref.} and P_{D Ref.}) of the reference Ship-2 computed using respectively the BEM/RANSE coupled solver and the fully RANSE analyses

analyzed and automatically modified based on the feedback of previous calculations to comply with the design objectives and constraints, which in this case are only of geometrical type. For the estimation of the quantities of interest, namely the delivered power, actuator disk calculations and a dedicated BEM/RANSE coupled method have been respectively developed to comply with the need of accurate predictions in a computationally efficient way. Surrogate models were also applied to a second design activity with the aim to verify the feasibility of a fast design workflow employing Kriging

approximations in place of “true” calculations of the quantities of interests throughout the design process. In both cases the extensive exploration of the design space, possible thanks to the design frameworks specifically developed, allowed for substantial energy savings also for these particular hulls, that are not the usual full-blocked ships for which this type of appendages already demonstrate its effectiveness. The versatility of the design method appears also in the possibility of monitoring side effects like the risk of cavitation, which were explicitly and quantitatively accounted throughout the

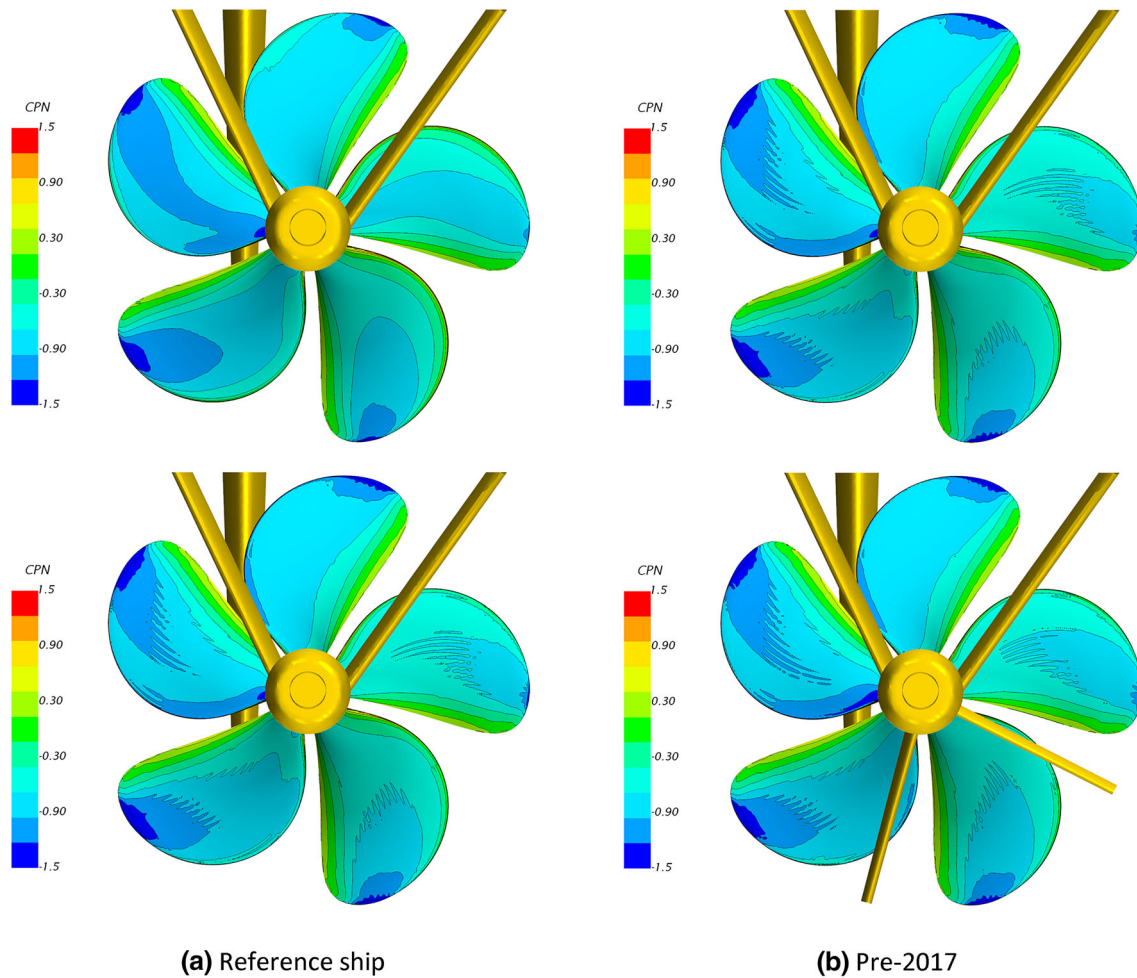


Fig. 23 Optimal Pre-Swirl fins arrangement and pressure coefficient (C_{PN}) on the starboard propeller blades, seen from bow (suction side). Comparison with the reference configuration of Ship-2. From top to bottom, ship speeds of 14 and 17 kn. **a** Reference ship and **b** Pre-2017

design process. The validation with fully resolved propeller RANSE analyses confirmed the validity of the designs that provide savings between 2 and 3% for the entire range of functioning conditions under investigation.

Author contributions All authors contributed to the study conception and design. Conceptualization and Methodology were performed by SG. Material preparation, data collection, software and analysis were performed by MM. The first draft of the manuscript was written by SG and all authors commented on previous versions of the manuscript. All authors read and approved the final manuscript.

Funding Open access funding provided by Università degli Studi di Genova within the CRUI-CARE Agreement. This research activity was co-funded by “Programma Operativo Por FSE Regione Liguria 2014–2020” under grant RLOF18ASSRIC/4/1. This research was supported by Azimut-Benetti that kindly provided data for the referenced test cases geometries.

Declarations

Competing interest The authors declare that they have no known competing financial interests or personal relationships that could have appeared to influence the work reported in this paper.

Open Access This article is licensed under a Creative Commons Attribution 4.0 International License, which permits use, sharing, adaptation, distribution and reproduction in any medium or format, as long as you give appropriate credit to the original author(s) and the source, provide a link to the Creative Commons licence, and indicate if changes were made. The images or other third party material in this article are included in the article’s Creative Commons licence, unless indicated otherwise in a credit line to the material. If material is not included in the article’s Creative Commons licence and your intended use is not permitted by statutory regulation or exceeds the permitted use, you will need to obtain permission directly from the copyright holder. To view a copy of this licence, visit <http://creativecommons.org/licenses/by/4.0/>.

References

- Andersen P, Andersen SV, Bodger L, Friesch J, Kappel JJ (2000) Cavitation considerations in the design of Kappel propellers. In: NCT'50. International conference on propeller cavitation, Newcastle, UK
- Carlton J (2007) Marine propellers and propulsion. Butterworth-Heinemann, Amsterdam
- Eça L, Hoekstra M (2014) A procedure for the estimation of the numerical uncertainty of CFD calculations based on grid refinements studies. *J Comput Phys* 262:104–130
- Esteco (2017) modeFRONTIER Users' manual. ESTECO SpA, an Italian-based software/CAE society
- Forrester A, Sobester A, Keane A (2008) Engineering design via surrogate modelling: a practical guide. Wiley, Hoboken
- Furcas F, Gaggero S (2021) Pre-swirl stators design using a coupled BEM-RANSE approach. *Ocean Eng* 222:108579. <https://doi.org/10.1016/j.oceaneng.2021.108579>
- Furcas F, Vernengo G, Villa D, Gaggero S (2020) Design of Wake Equalizing Ducts using RANSE-based SBDO. *Appl Ocean Res* 97:102087. <https://doi.org/10.1016/j.apor.2020.102087>
- Gaggero S (2020) Numerical design of a RIM-driven thruster using a RANS-based optimization approach. *Appl Ocean Res* 94:101941. <https://doi.org/10.1016/j.apor.2019.101941>
- Gaggero S, Villa D, Viviani M (2017) An extensive analysis of numerical ship self-propulsion prediction via a coupled BEM/RANS approach. *Appl Ocean Res* 66:55–78. <https://doi.org/10.1016/j.apor.2017.05.005>
- Gaggero S, Dubbioso G, Villa D, Muscari R, Viviani M (2019) Propeller modeling approaches for off-design operative conditions. *Ocean Eng* 178:283–305. <https://doi.org/10.1016/j.oceaneng.2019.02.069>
- Gaggero S, Villa D, Viviani M (2014) An Investigation on the discrepancies between RANSE and BEM approaches for the prediction of marine propeller unsteady performances in strongly non-homogeneous wakes. In: International conference on offshore mechanics and arctic engineering. American Society of Mechanical Engineers, San Francisco, California, USA. <https://doi.org/10.1115/OMAE2014-23831>
- Gaggero S, Gaggero T, Tani G, Vernengo G, Viviani M, Villa D (2018) Ship self-propulsion performance prediction by using OpenFOAM and different simplified propeller models. In: Progress in maritime technology and engineering: proceedings of the 4th international conference on maritime technology and engineering (MARTECH 2018), May 7–9, 2018, Lisbon, Portugal, CRC Press, p 195
- International Maritime Organization – Part a (IMO) (2009a) Interim guidelines for voluntary verification of the energy efficiency design index. MEPC.1/Circ.682, 17 August 2009a. IMO, London
- International Maritime Organization – Part b (IMO) (2009b) Guidelines for voluntary use of the ship energy efficiency operational indicator. MEPC.1/Circ. 684, 17 August 2009b. IMO, London
- International Maritime Organization (2014) Annex 5, Resolution MEPC.245(66). Guidelines on the Method of Calculation of the Attained Energy Efficiency Design Index (EEDI) for New Ships. London
- Kim K, Leer-Andersen M, Werner S, Orych M, Choi Y (2013) Hydrodynamic optimization of pre-swirl stator by CFD and model testing. *Int Shipbuild Prog* 60(1–4):233–276. <https://doi.org/10.3233/ISP-130092>
- Kim MC, Chun HH, Kang YD (2004) Design and experimental study on a new concept of preswirl stator as an efficient energy-saving device for slow speed full body ship. In: SNAME annual meeting.
- Kinnas SA, Hsin CY (1992) Boundary element method for the analysis of the unsteady flow around extreme propeller geometries. *AIAA J* 30(3):688–696. <https://doi.org/10.2514/3.10973>
- Koushan K, Krasilnikov V, Nataletti M, Sileo L, Spence S (2020) Experimental and numerical study of pre-swirl stators PSS. *J Mar Sci Eng* 8(1):47. <https://doi.org/10.3390/jmse8010047>
- Lammeren WV (1949) Enkele Constructies ter Verbetering van het Rendement van de Voortstuwing. Nederlands Scheepsbouwkundig Proefstation, Wageningen, Report No. 77, Publicatie in: Schip en Werf, No. 7, 1949, Wyt-Rotterdam
- Lophaven SN, Nielsen HB, Søndergaard J (2002) DACE: a Matlab kriging toolbox. IMM, Informatics and Mathematical Modelling, The Technical University of Denmark, Denmark
- Morino L, Chen LT, Suci EO (1975) Steady and oscillatory subsonic and supersonic aerodynamics around complex configurations. *AIAA J* 13(3):368–374. <https://doi.org/10.2514/3.49706>
- Nielsen JR, Jin W (2019) Pre-swirl fins adapted to different operation conditions. In: Proceedings of the 6th international symposium on marine propulsors
- Ouchi K, Ogura M (1988) A research and development of PBCF (propeller boss cap fins), improvement of flow from propeller boss. *J Soc Nav Archit Jpn* 163:66–78. <https://doi.org/10.2534/jjasnaoe1968.1988.66> (in Japanese)
- Prins HJ, Flikkema MB, Schuiling B, Xing-Kaeding Y, Voermans AAM, Müller M, Coache S, Hasselaar TWF, Paboef S (2016) Green retrofitting through optimisation of hull-propulsion interaction—GRIP. *Transp Res Procedia* 14:1591–1600. <https://doi.org/10.1016/j.trpro.2016.05.124>
- Schuiling B, van Terwisga T (2017) Hydrodynamic working principle of energy saving devices in ship propulsion system. *Int Shipbuild Prog* 63(3–4):255–290. <https://doi.org/10.3233/ISP-170134>
- Siemens PLM (2017) StarCCM+ Users' manual v 1204. Siemens PLM, Plano
- Starke AR, Bosschers J (2012) Analysis of scale effects in ship powering performance using a hybrid RANS-BEM approach. In: 29th Symposium on Naval Hydrodynamics (ONR), Gothenburg, Sweden, 2012, 2012
- Streckwall H, Xing-Kaeding Y (2017) On the working principle of pre-swirl stators and on their application benefit and design targets. *Int Shipbuild Prog* 63(3–4):87–107. <https://doi.org/10.3233/ISP-170124>
- Villa D, Gaggero S, Gaggero T, Tani G, Vernengo G, Viviani M (2019) An efficient and robust approach to predict ship self-propulsion coefficients. *Appl Ocean Res* 92:101862. <https://doi.org/10.1016/j.apor.2019.101862>

Publisher's Note Springer Nature remains neutral with regard to jurisdictional claims in published maps and institutional affiliations.